JACS
JOURNAL OF THE AMERICAN CHEMICAL SOCIETY
Article
pubs.acs.org/JACS

Fundamental Molecular Mechanism for the Cellular Uptake of Guanidinium-Rich Molecules

Henry D. Herce,[†,‡] Angel E. Garcia,*[,†] and M. Cristina Cardoso[‡]

[†]Department of Physics, Applied Physics and Astronomy and Center for Biotechnology and Interdisciplinary Studies, Rensselaer Polytechnic Institute, Troy, New York 12180, United States

[‡]Department of Biology, Technische Universität Darmstadt, 64287 Darmstadt, Germany

Supporting Information

ABSTRACT: Guanidinium-rich molecules, such as cell-penetrating peptides, efficiently enter living cells in a non-endocytic energy-independent manner and transport a wide range of cargos, including drugs and biomarkers. The mechanism by which these highly cationic molecules efficiently cross the hydrophobic barrier imposed by the plasma membrane remains a fundamental open question. Here, a combination of computational results and in vitro and live-cell experimental evidence reveals an efficient energy-independent translocation mechanism for arginine-rich molecules. This mechanism unveils the essential role of guanidinium groups and two universal cell components: fatty acids and the cell membrane pH gradient. Deprotonated fatty acids in contact with the cell exterior interact with guanidinium groups, leading to a transient membrane channel that facilitates the transport of arginine-rich peptides toward the cell interior. On the cytosolic side, the fatty acids become protonated, releasing the peptides and resealing the channel. This fundamental mechanism appears to be universal across cells from different species and kingdoms.

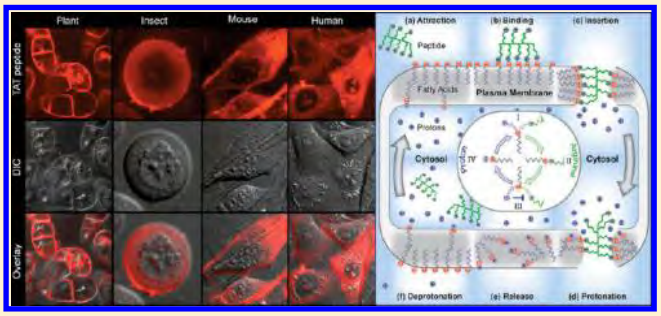

1. INTRODUCTION

Cell-penetrating peptides are short, usually arginine-rich amino acid sequences that are capable of transporting a wide range of biomolecules into virtually any living cell type.[1−8] There is abundant evidence that these peptides are able to directly translocate across the plasma membrane in an energy-independent and non-endocytotic manner, gaining free access to the cytosol and nucleus.[9−13] This challenges the fundamental concept that charged molecules cannot spontaneously diffuse across the cell membrane. The mechanism behind this puzzling effect follows three essential steps: (a) peptide binding to plasma membrane components; (b) spontaneous peptide absorption across the hydrophobic barrier imposed by the plasma membrane; and (c) breakage of the strong ionic binding between the peptide and the membrane when the peptide reaches the cytosol.

Arginine-rich peptides (RRPs) have strong affinities for multiple negatively charged plasma membrane groups. This affinity is so strong that removal of membrane-bound peptides requires enzymatic degradation of the peptides and the addition of strong counterions such as heparin to the wash solution.[14] However, it remains unclear whether any of these multiple cell membrane components could efficiently mediate the absorption of the RRPs into the hydrophobic core of the plasma membrane. It has been suggested that some membrane components could form stable complexes with RRPs, mediating their absorption into the core of the plasma membrane by forming either inverted micelles[15−17] or transient channels.[18−27] In both models, the peptides would reach the intracellular side of the cell membrane strongly bound to the cell membrane. Therefore, even if any of these mechanisms is right, there should be in place a common cellular mechanism to release these peptides from the cell membrane after they reach the cytosol.

Herein is described a complete cellular uptake mechanism for RRPs based on the ubiquitous interplay between two universal cell components: fatty acids and the plasma membrane pH gradient. We propose that at high pH fatty acids bind extracellular RRPs, mediate their membrane transport, and release them into the lower-pH environment of the cytosol. In vitro experiments presented here show all of the major steps of this mechanism. Computational results show that deprotonated fatty acids reduce the free energy of insertion of RRPs into model phospholipid bilayers and that this insertion leads to the formation of a channel across the lipid bilayer. Accordingly, live-cell experiments show that both the extracellular pH and the cell membrane fatty acid content modulate the cell transduction of RRPs into living cells. Furthermore, this mechanism describes the puzzling cell uptake differences observed between polyarginine and polylysine peptides. Finally, peptide uptake observations in multiple cell lines and the universality of the elements involved in this model (fatty acids

Received: July 30, 2014
Published: November 18, 2014

 © 2014 American Chemical Society dx.doi.org/10.1021/ja507790z | J. Am. Chem. Soc. 2014, 136, 17459−17467

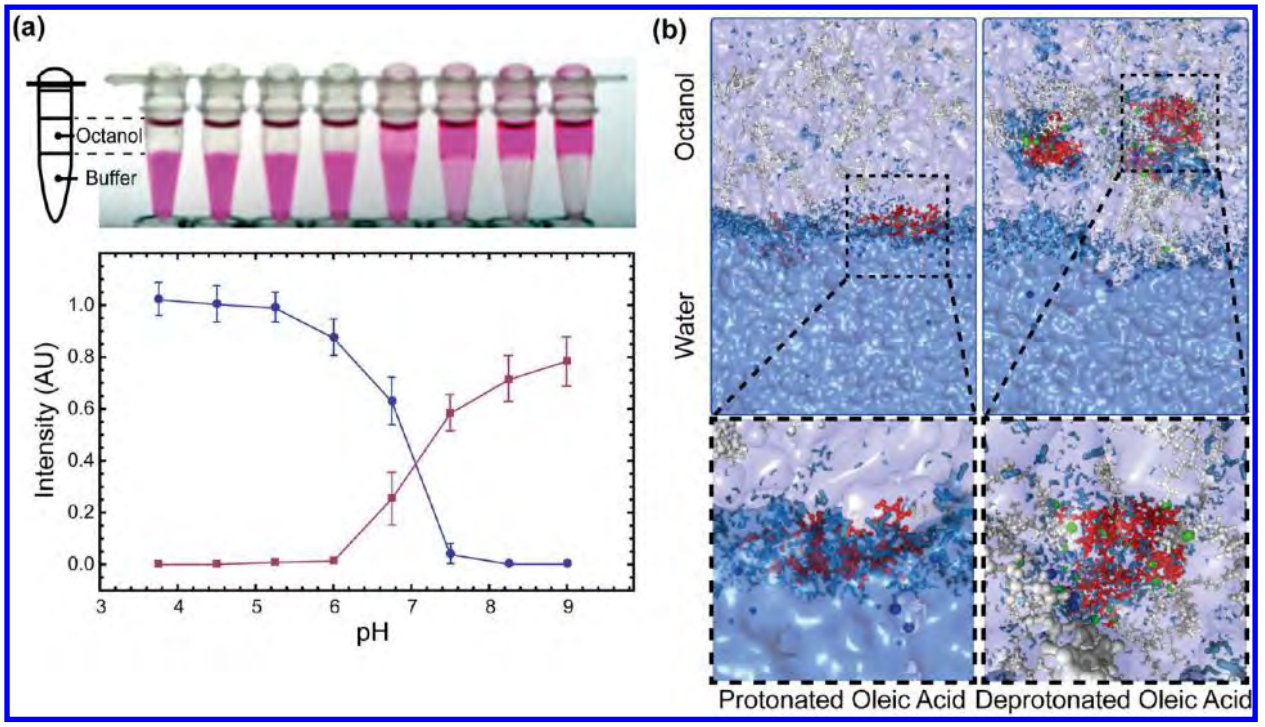

Figure 1. Within a physiological pH range, arginine-rich peptides can partition into an aqueous buffer at low pH and a hydrophobic environment at high pH. (a) Photograph showing that at pH less than 6.75 the TAT peptide (10 μM), labeled with TAMRA, partitions mainly into the aqueous phase, while at any pH higher than 6.75 the TAT peptide partitions mainly into the phase composed of octanol and 1% oleic acid. The plot shows the fluorescence emission of the peptide in each phase for each pH. While arginine and lysine amino acids do not change their protonation state within this range, fatty acids change from being neutral (protonated) at low pH to negatively charged (deprotonated) at high pH. (b) Snapshots after 300 ns molecular dynamics simulations of systems composed of 16 000 octanol molecules (represented with a white transparent surface), 64 protonated (left) or deprotonated (right) oleic acid molecules (the carbon chains of oleic acids are colored in white, while oxygens of protonated oleic acid are colored in gray and oxygens of deprotonated oleic acid are colored in green), four peptides (in red), 24 000 water molecules (blue surface; water molecules within 3 Å of any atom of the peptide or octanol or fatty acids are explicitly shown in blue), and chloride (left) or potassium (right) ions (in blue) to neutralize the system. When the fatty acids are protonated, the TAT peptides are excluded from the octanol phase, while when the fatty acids are deprotonated, the peptides partition in the octanol phase surrounded by fatty acids and water in a structure that resembles an inverted micelle.

and the cell pH gradient) suggest that this mechanism is universal across cells from different species and kingdoms.

2. RESULTS AND DISCUSSION

2.1. Protonation State of Fatty Acids Modulates RRP Binding. The central hypothesis of this work is that fatty acids can simultaneously mediate RRP membrane binding, membrane insertion, and cytosolic release. We postulate that this process is triggered by the pH gradient across the plasma membrane.

A simple in vitro model system to test this hypothesis is to study the distribution of RRPs between an aqueous buffer and octanol. Figure 1a shows a photograph displaying an aqueous buffer at different pHs in contact with an octanol phase containing 1% oleic acid. At pH less than 6.75, the TAT peptide (an RRP derived from the HIV-1 TAT protein) partitions mainly into the aqueous phase, while at any pH larger than 6.75, the TAT peptide is absorbed into the octanol phase. The plot shows the fluorescence emission intensity of the peptide labeled with TAMRA in each phase and at each pH value of the buffer. This indicates that fatty acids change from being neutral (protonated) at low pH to negatively charged (deprotonated) at high pH. Remarkably, the peptide absorption into the hydrophobic phase can be modulated within a physiological range very close to the extra- and intracellular pH in mammalian cells.

Figure S1 in the Supporting Information shows as a control this partition for the TAMRA dye alone, which partially partitions into the octanol phase at pH lower than 6, while for any higher pH the dye partitions only into the aqueous phase. This is the opposite behavior as when the dye is coupled to the TAT peptide (Figure 1a), indicating that the peptides drive the partition of the dyes into the aqueous phase at low pH and into the hydrophobic phase at high pH.

To obtain structural information on the peptides absorbed into the hydrophobic phase, we performed molecular dynamics simulations. Figure 1b shows a system composed of octanol, protonated (left) or deprotonated (right) oleic acid molecules, peptides, water, and chloride or potassium ions to balance the charges. We can see that when the fatty acids are protonated, the TAT peptides are excluded from the octanol phase, while when the fatty acids are deprotonated, the peptides partition into the octanol phase, forming a hydrophobic complex surrounded by fatty acids with a hydrophilic interior composed of water, ions, and the peptide. Therefore, peptides can be absorbed into octanol by forming structures with fatty acids that resemble inverted micelles with the polar groups in the interior of the structure.

We next explored whether other groups and hydrophobic environments would be able to modulate the absorption of arginine-rich peptides within a physiological pH range.

dx.doi.org/10.1021/ja507790z | J. Am. Chem. Soc. 2014, 136, 17459−17467

2.2. Fatty Acids Ubiquitously Modulate the Absorption of RRPs into a Hydrophobic Environment within a Physiological pH Range. In the absence of oleic acid, TAT does not enter the hydrophobic phase, as shown in Figure 2a. This indicates that the pH change only modulates the protonation of fatty acids. The pK_a of simple carboxyl acids is around 4.5, such as formic acid (pK_a = 3.77) or acetic acid (pK_a = 4.76), while the pK_a of fatty acids in pure monolayers is around 10. The pK_a, or apparent pK_a, of fatty acids depends on several factors such as the degree, type, and position of unsaturation and the local environment,[28] and it has recently been shown that in cells this value could be shifted toward a physiological pH range.[29] On the other hand, the protonation state of guanidinium groups is very stable even in hydrophobic environments.[30]

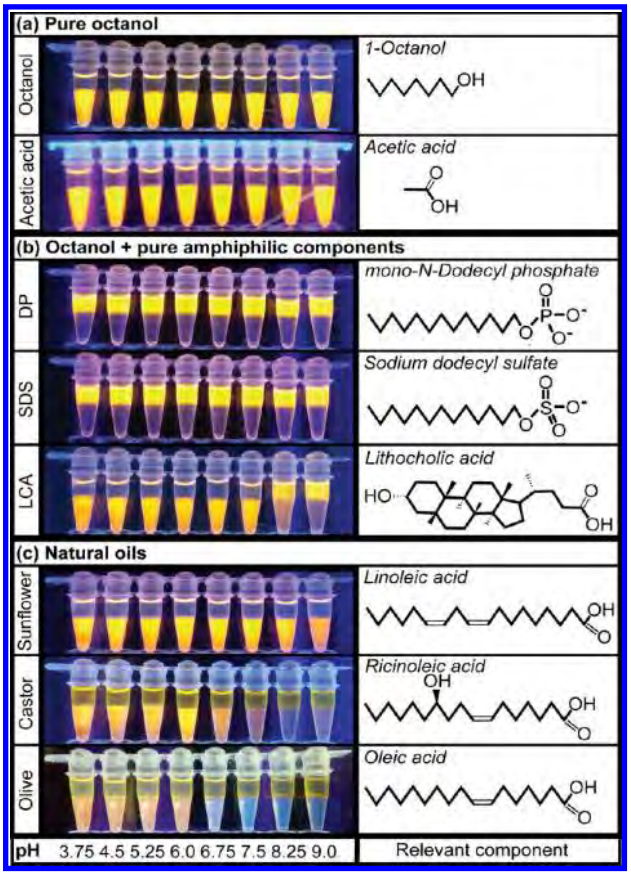

Figure 2. Fatty acids ubiquitously modulate the partition of arginine-rich peptides within a physiological pH range. In the left column are shown snapshots of microcentrifuge tubes containing the different hydrophobic phases in contact with the aqueous buffers at different pHs. The right column shows the structures of the relevant components. The TAT peptide was labeled with TAMRA and excited with UV light (280 nm) to facilitate the visualization of the peptide distribution. (a) In the absence of carboxylic groups coupled to hydrophobic moieties, such as fatty acids, the TAT peptide does not partition into octanol. (b) In the presence of hydrophobic compounds containing phosphate and sulfur groups (100 μM in octanol) the TAT peptide (10 μM) partitions into the hydrophobic phase at every pH. These groups could help attract the peptides toward the plasma membrane. However, these groups fail to provide a mechanism for cytosolic release of membrane-bound peptides. On the other hand, other hydrophobic molecules containing carboxyl groups, such as lithocholic acid, display behavior similar to that of oleic acid, although in this case the deprotonation is shifted toward higher pH. (c) Partition of the TAT peptide into three distinct types of natural vegetable oils: sunflower oil, castor oil, and olive oil. Vegetable oils are rich in fatty acids. However, most of these fatty acids are not free but instead form triglycerides, which lack free carboxyl groups essential for the binding of RRPs.

It has been speculated that membrane phosphate and sulfur groups might be critical for the cellular uptake of RRPs, but it can be seen in Figure 2b that although these groups bind to RRPs, they remain bound at every pH. These groups could help attract the peptides toward the plasma membrane. However, they fail to provide a mechanism for cytosolic release of membrane-bound peptides. Furthermore, at the plasma membrane these groups are usually part of more complex molecules such as plasma membrane phospholipids that are more rigid and less likely to flip across the bilayer than simple fatty acids, thus providing stability to the plasma membrane. At high concentrations, these peptides can also penetrate and change the structure of phospholipid membranes,[27] and their toxicity at high concentrations might be a consequence of permanently destabilizing the phospholipid bilayer. All of these factors make less favorable the membrane absorption, translocation, and release of RRPs by complexation with plasma membrane components containing phosphate or sulfur groups. Figure 2b also shows that carboxyl groups present in other types of amphiphilic molecules, such as lithocholic acid, display behavior similar to that of oleic acid, although the deprotonation in this case is shifted to a higher pH, suggesting that other molecules containing a hydrophobic moiety coupled to carboxyl groups could analogously modulate the absorption of arginine-rich molecules. This could help explain recent works that have highlighted the specific role of pyrenebutyrate, originally suggested by Sakai and Matile,[15] as an enhancer of the cellular uptake of RRPs.[31,32] This particular enhancer is composed of a carboxyl group (from the butyric acid part of the molecule) followed by a hydrophobic structure (mainly from the aromatic pyrene part).

To explore these effects in richer hydrophobic environments, we also studied the partition of RRPs into three distinct types of natural vegetable oils: sunflower oil, castor oil, and olive oil. Vegetable oils are rich in fatty acids. However, most of these fatty acids are not free but instead form triglycerides, which lack free carboxyl groups essential for the binding of RRPs. We can see in Figure 2c that sunflower oil displays a behavior consistent with a composition of only triglycerides, displaying no absorption of the TAT peptide in the hydrophobic phase. Castor oil behaves as also having free fatty acids, showing an absorption behavior similar to that of oleic acid (Figure 1a). Olive oil displays absorption of the TAT peptide at the interface at every pH, revealing the presence of phospholipids.[33] This absorption remains constant until pH 6, followed by a clear increase in absorption at higher pHs produced by the additional presence of free fatty acids.

We next adapted the previous in vitro setup to test whether this mechanism would allow the spontaneous transfer of RRPs from a high- to a low-pH buffer across a hydrophobic barrier.

2.3. Fatty Acids Can Transport RRPs across a Hydrophobic Barrier. The proton gradient across the cell membrane can regulate fatty acid protonation and drive the cellular uptake of RRPs. Therefore, we asked whether this effect could be captured in an analogous in vitro assay. This assay should display the transport of cell-penetrating peptides from a high-pH buffer to a low-pH buffer across a hydrophobic barrier. Figure 3 shows that RRPs indeed diffuse across the octanol

dx.doi.org/10.1021/ja507790z | J. Am. Chem. Soc. 2014, 136, 17459−17467

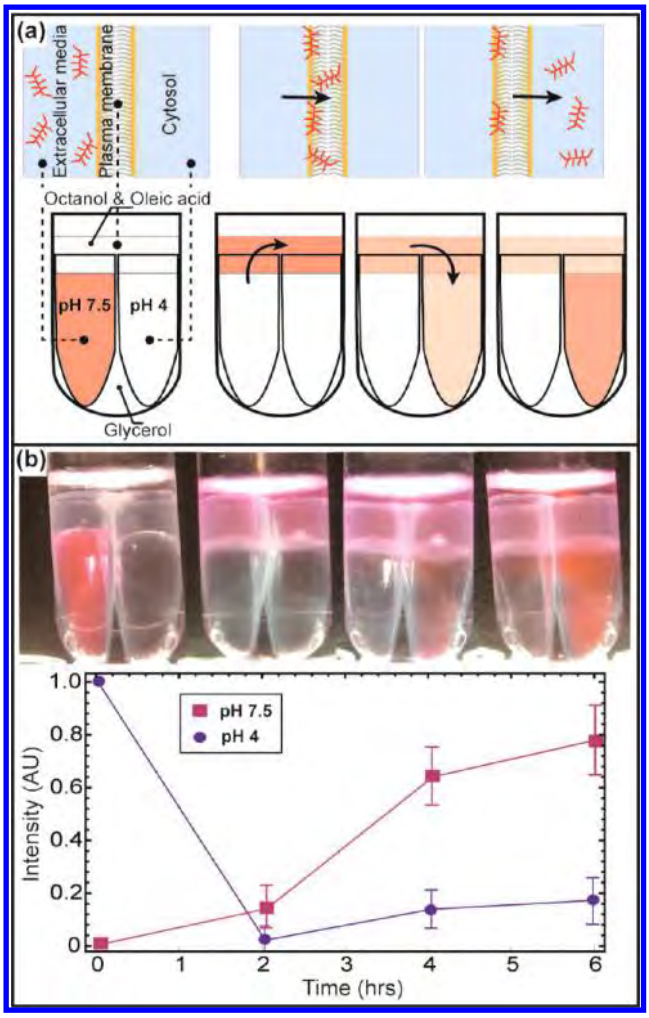

Figure 3. Arginine-rich cell-penetrating peptides can diffuse across a hydrophobic environment from a high- to a low-pH buffer in the presence of fatty acids. (a) Cartoon description of the cellular analogue of the in vitro setup, in which arginine-rich peptides are added to the extracellular medium at higher pH and diffuse across the membrane barrier toward the interior of cells at lower pH. The in vitro setup consists of two compartments at pH 7.5 and 4 connected by a layer of octanol and 1% oleic acid. The peptides were added to the high-pH compartment (pH 7.5), and they initially diffused into the hydrophobic phase and then at a lower rate into the low-pH buffer (pH 4). (b) Photographs of the setup and a plot of the peptide distribution (fluorescence emission) at different times. After 6 h, the peptides were mostly distributed between the octanol phase and the low-pH chamber.

hydrophobic barrier in the presence of fatty acids from a high-pH to a low-pH buffer. Figure 3a shows a cartoon illustration of the in vitro setup and its cellular analogue. The in vitro setup consists of two compartments at pH 7.5 and 4 connected by a layer of octanol with 1% oleic acid. Cells actively control the pH gradient across the plasma membrane, while in this experimental set up the pH is not actively maintained in each chamber. This could potentially lead to a fast pH equilibration between the two chambers as a consequence of the fatty-acid-mediated transfer of protons. Therefore, we chose a lower pH for the trans compartment than in the cytosol to ensure that the pH gradient between the two compartments would be maintained throughout the experiment. The TAT peptides were added to the pH 7.5 buffer. Figure 3b displays photographs of the setup at 2 h intervals and a plot of the relative fluorescence intensity in each buffer at each time point. After 2 h the peptides get absorbed initially into the hydrophobic phase and then at a lower rate diffuse into the low-pH chamber. After 6 h, the peptides are mostly distributed between the octanol phase and the low-pH buffer. Therefore, fatty acids can mediate the transport of RRPs across a hydrophobic environment from a high- to a low-pH buffer, resembling the cellular uptake of RRPs. Furthermore, the low-pH buffer can be considered a trap for the peptides, as the peptides diffuse in one direction. The diffusion of the peptides across the hydrophobic environment is primarily determined not by the peptide concentration but instead by the proton concentration. This correlates with the observation that RRPs diffuse toward the interior of cells and that after the extracellular peptides are washed away the internalized peptides remain trapped in the cells.

We next asked how the protonation of fatty acids affects the absorption of RRPs in phospholipid bilayers.

2.4. Fatty Acids Lower the Plasma Membrane Energetic Barrier for RRPs. To understand how fatty acids affect the peptide−membrane interaction in more detail, we computed the free energy profiles for the insertion of a TAT peptide into model phospholipid bilayers composed of a mixture of 1,2-dioleoyl-*sn*-glycero-3-phosphocholine (DOPC) and oleic acid. Umbrella sampling was used to enhance the sampling along the free energy barrier imposed by the lipid bilayer. Essentially, an external harmonic potential was introduced, restraining the peptide at multiple positions across the bilayer. The contribution of this bias to the free energy was consistently removed using the WHAM method to obtain the free energy required to insert the peptide into the bilayer.[34−36] Figure 4 shows the structures and free energy profiles of three systems composed of a TAT peptide, water molecules, and a lipid bilayer made of DOPC and oleic acid molecules. Figure 4a presents snapshots of the atomic conformations of the three systems studied, with the peptide at the center of the bilayer. These structures show that in the presence of deprotonated fatty acids the peptide's charged residues are screened by deprotonated fatty acids that easily insert into the center bilayer. On the other hand, in the absence of deprotonated fatty acids the arginine and lysine residues cannot be easily screened at the center of the bilayer, leading the peptide to acquire an extended conformation to reach the phosphate groups of the more rigid phospholipids on the surface. Movies S1−S3 in the Supporting Information show structural changes as the TAT peptide is inserted into the bilayer and the relative free energy along this path for each case. These free energies are plotted in Figure 4b, where it can be seen that the addition of protonated fatty acids to the bilayer reduces by half the reported[36] free energy of insertion of the TAT peptide into pure DOPC bilayers. It can be seen that when all of the fatty acids are deprotonated, the free energy barrier is further reduced to 25 kJ/mol. This reduction is a consequence of efficient screening of the arginine and lysine residues by deprotonated fatty acids. This energetic barrier could be further reduced by the cell transmembrane potential,[16,37,38] which is not necessary for the transport across octanol.

It has been proposed that a possible mechanism of insertion of RRPs into the core of the bilayer might involve the formation of reverse micelles[39,40] with RRPs surrounded by ambiphilic counterions, resembling the structure shown in Figure 1b. However, we can see that in three independent

dx.doi.org/10.1021/ja507790z | J. Am. Chem. Soc. 2014, 136, 17459−17467

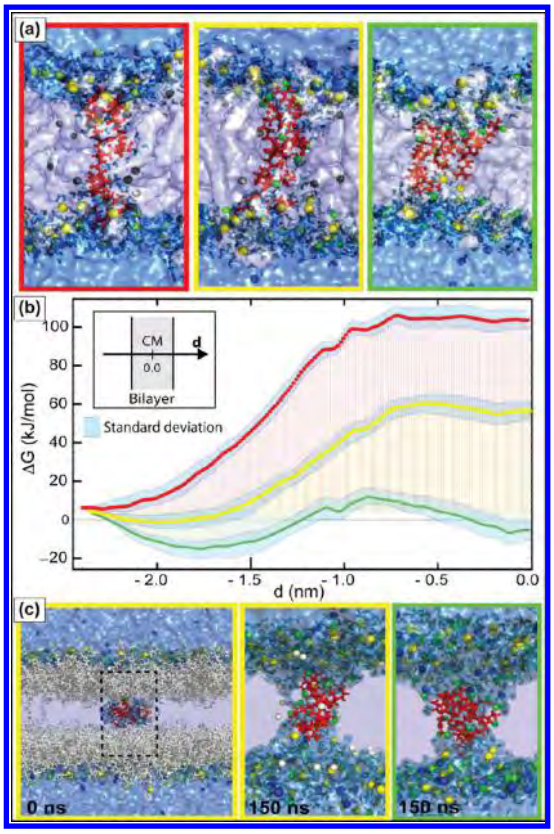

Figure 4. Structural analysis and free energy computations for insertion of the TAT peptide into phospholipid bilayers containing protonated and deprotonated fatty acids using molecular dynamics simulations. (a) Molecular conformations of the systems with the peptide constrained at the center of the bilayer. The systems are composed of a TAT peptide, 8700 water molecules, 68 DOPC molecules, and 48 oleic acid molecules (all protonated in red, half deprotonated in yellow, and all deprotonated in green). The systems are neutralized with the addition of potassium or chloride ions. Water is represented by a blue surface, with water molecules less than 3 Å from any atom of the peptide or lipid bilayer explicitly drawn in blue. DOPC and oleic acid molecules are shown with a white surface. Phosphate atoms are shown in yellow, protonated and deprotonated fatty acid carboxyl groups are shown in gray and green, respectively, and the TAT peptide is shown in red. (b) Free energy profiles as functions of the distance of the center of mass of the TAT peptide from the center of mass of the lipid bilayer. The total computed time for each free energy calculation profile was expanded to 10 μs. (c) To see whether an inverted-micelle-like structure would be stable at the center of the bilayer, we increased the bilayer size by a factor of 4 and inserted a single TAT peptide surrounded by water and oleic acid molecules that was previously equilibrated within a mixture of octanol and deprotonated fatty acids (Figure 1b). The final system was composed of 272 DOPC molecules, 200 oleic acid molecules, potassium counterions, 34 800 water molecules, and a TAT peptide. The peptide–fatty acid complex obtained from the simulation shown in Figure 1b was placed in the middle of the bilayer. The layers of the bilayer were separated, leaving significant space between the complex hydrophobic core and the surface of the bilayer, and from this conformation the systems relaxed to equilibrium for 150 ns at constant pressure. In the two cases tested, the initial structure resembling a reverse micelle transformed into a water-filled channel.

simulations (Figure 4a), when a peptide is inserted in the center of the bilayer, the lipid bilayer forms a water-channel structure.[18−20] To be sure that the system was not biased toward channel formation by the computed system size or the initial structure, we performed a new computation in which the system was enlarged and the initial structure was biased toward the formation of an inverted-micelle-like structure in the center of the bilayer. In Figure 4c, we increased the bilayer size by a factor of 4 and inserted a single TAT peptide surrounded by water and deprotonated oleic acid using an initial structure from the simulations in Figure 1b resembling an inverted micelle. The peptide–fatty acid complex obtained from the simulation shown in Figure 1b was placed in the middle of the bilayer. The layers of the bilayer were separated, leaving significant space to fit the inverted-micelle-like structure, and from this conformation the systems relaxed at constant pressure to their final volume. In every case, the systems relaxed spontaneously to form a channel. This further supports that the insertion of RRPs into lipid bilayers leads to the formation of channels.[18−20]

Interestingly, it can also be observed that protonated fatty acids rapidly flip from one side of the bilayer to the other, while deprotonated fatty acids do not flip within this time scale. If the extracellular pH is much higher than the intracellular pH, any intracellular fatty acid that becomes protonated in the cytosol would rapidly flip, get deprotonated, and remain captured in the extracellular layer of the cell membrane. This implies that increasing the extracellular pH would greatly increase the number of deprotonated fatty acids in contact with the external side of the plasma membrane, leading to an enhancement of the cellular uptake of RRPs.

Cells actively control the intracellular pH, keeping it near neutral pH, but the extracellular pH can be chemically controlled. Therefore, we next asked whether altering the extracellular pH would modulate the uptake of RRPs into living cells consistently with the previous in vitro and molecular dynamics observations.

2.5. Extracellular Proton Density Modulates the Cellular Uptake of RRPs. Fatty acids are an integral part of all known cells. If this mechanism is also present in cells, then raising (lowering) the extracellular pH should enhance (reduce) the transduction of these peptides. Therefore, as shown in Figure 5 and movies S4–S9 in the Supporting Information, we compared the uptake of the TAT peptide when the extracellular pH was chemically controlled at different values. In most mammalian cells, the extracellular pH is close to 7.4. Therefore, we studied the peptide uptake in HeLa cells with the extracellular pH kept at 6, 7.5, and 9 using a HEPES buffer. Figure 5 shows time-lapse confocal microscopy snapshots of the uptake of the TAT peptide in living cells. While at this TAT peptide concentration (2 mM) there was no uptake at pH 6 and 7.5, most of the cells kept at pH 9 displayed significant uptake within this time interval (30 min). We also measured the change in the average fluorescence intensity of the entire image minus the background fluorescence (Figure 5), and we can see that at pH 6 and 7.5 this value remains negative, indicating that the concentration of membrane-bound and/or intracellular peptide is less than that in the extracellular medium, while at pH 9 the curve is positive, indicating clear cellular uptake.

This experiment was performed using an objective with 20× magnification, allowing the simultaneous visualization of several cells in the field of view. At this magnification it was difficult to resolve clearly whether the increase in fluorescence was correlated with cellular uptake and/or membrane-bound peptides. Therefore, to be able to differentiate intracellular from membrane-bound peptides within the same field of view,

dx.doi.org/10.1021/ja507790z | J. Am. Chem. Soc. 2014, 136, 17459−17467

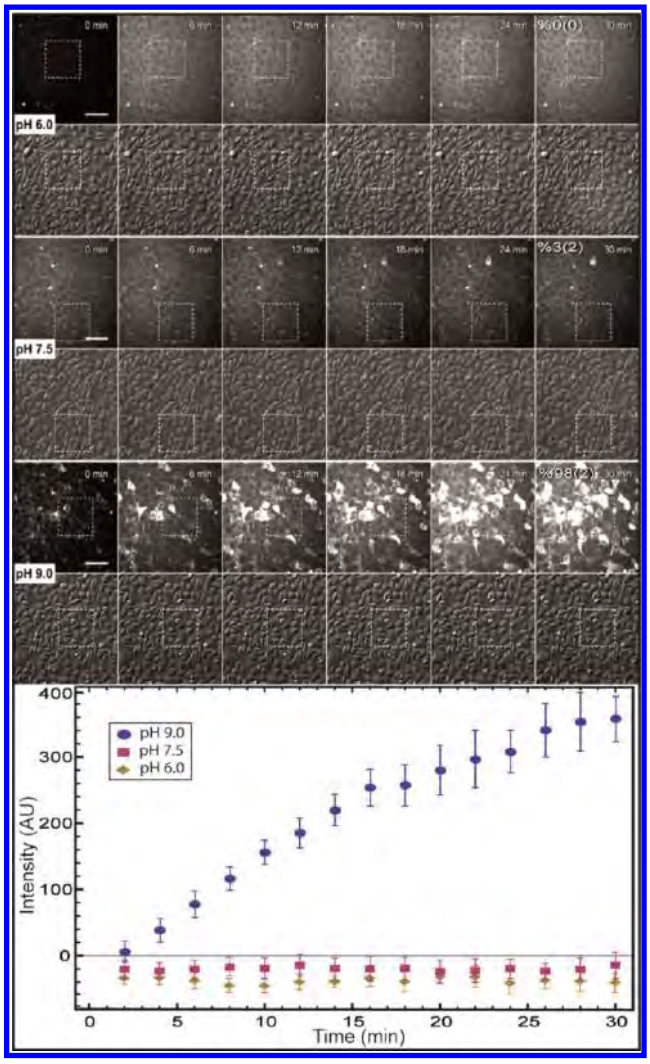

Figure 5. Increasing the extracellular pH consistently increases the transduction efficiency of arginine-rich peptides. Time-lapse fluorescence images show the TAT (2 μM) uptake in living cells at pH 6, 7.5, and 9. The lower plot shows the averages (over three independent repetitions) of the overall fluorescence intensity minus the background intensity and the standard errors of the mean as functions of time. After 30 min the fluorescence increased several-fold at pH 9 relative to pH 6 and 7.5. The images were acquired using an objective with 20× magnification. In this case, the membrane-bound peptide cannot be separated from the internalized peptide. To measure more strictly the free intracellular distributed peptide and compare it with these results, we simultaneously imaged the cells in the dotted regions using an objective with 60× magnification (Figure S2 in the Supporting Information). We measured the fluorescence intensity at the nucleolus relative to the background fluorescence over time and found that the two measurements gave analogous results. Scale bars = 75 μm.

we switched to a 60× objective (Figure S2 in the Supporting Information) to capture higher-magnification images of the dotted regions indicated in Figure 5. The plot in Figure S2 shows the fluorescence intensity in the nucleus minus the extracellular background fluorescence intensity. It can be seen that the internalized TAT peptide in the nucleus accumulated mainly at the nucleolus, from which it becomes easy to recognize that this fluorescence signal was produced only by free peptides and not by peptides trapped in endosomes or bound to the cell plasma membrane. Movies S4–S9 in the Supporting Information show the uptake of 2 μM TAT peptide by HeLa cells at pH 6, 7.5, and 9 taken at 20× and 60× magnification. Cells were deprived of glucose and nutrients during peptide uptake, and no peptide trapped in endosomes was detected during this time. Cells tolerated these conditions, remaining viable. They preserved their morphology (as shown by differential interference contrast (DIC) images), remained enzymatically active (Figure S3 in the Supporting Information), and kept undergoing normal cell division (movie S10 in the Supporting Information).

We also tested the effect of the extracellular pH on the uptake of multiple RRPs with different lengths, structures, and chirality[8,41−43] using cell lines from different species and kingdoms (Figures S4–S9 in the Supporting Information). Increasing the extracellular pH resulted in an increase in cellular peptide uptake for all RRPs by all cell lines. Consistently in all of the cell lines studied here, at pH 6 there was almost no uptake of the peptide compared with pH 7.5 and 9. The fact that this behavior is common to cells from widely separated evolutionary organisms highlights the universality of the underlying mechanism that drives the cellular uptake of RRPs.

We asked next whether enriching the cells with fatty acids would also increase the uptake of RRPs.

2.6. Fatty Acid Plasma Membrane Enrichment Enhances Uptake of RRPs. Incubating cells in a medium enriched with fatty acids can increase the cell content of fatty acids.[44,45] Therefore, we first incubated the cells in a medium rich in fatty acids for 5 min and then washed and incubated the cells in a buffer at pH 7.5 with different concentrations of the TAT peptide (10, 5, and 2.5 μM). The cells were then washed and medium plus calcein was added to monitor for enzymatic activity, and the cells were imaged. In Figure 6 it can be seen that fatty-acid-enriched cells display a much higher uptake efficiency than the control cells and that most of the cells are viable as indicated by their morphology and enzymatic activity.

Polyarginine peptides (>7 amino acids long) efficiently transduce into living cells. However, this is not the case for polylysine peptides.[41,46] This is an intriguing result since both arginine and lysine residues remain positively charged over a broad physiological pH range. Therefore, fatty acids could analogously mediate the transport of polylysine peptides. We next asked whether fatty acids would consistently capture these remarkable differences.

2.7. Fatty Acids Capture Differences between Polyarginine and Polylysine. If fatty acids indeed play an active role in the cellular uptake of RRPs, then they should also consistently show a clear selectivity for arginine over lysine amino acids, making this a sensible test for the mechanism proposed here. Therefore, we first looked at the structure and energetics of the interaction between arginine amino acids (or guanidinium groups) and lysine amino acids (or amino groups) with the deprotonated carboxyl group of oleic acid. Using molecular dynamics simulations (Figure 7a), we computed the free energy as a function of the distance between the carboxyl carbon of oleic acid and the carbon (nitrogen) atom of the guanidinium (amino) group. This calculation shows that as the guanidinium group approaches the carboxyl group it encounters a free energy barrier of 1.8 kJ/mol, and the energy gained upon binding is 8.5 kJ/mol. In contrast, the amino group encounters a much higher free energy barrier of 6.1 kJ/mol, and the binding energy gain is only 2.5 kJ/mol. Therefore, guanidinium groups encounter an energetic barrier more than 3 times weaker to bind fatty acids relative to amino groups, and the relative gain in energy is more than 3 times higher.

dx.doi.org/10.1021/ja507790z | J. Am. Chem. Soc. 2014, 136, 17459−17467

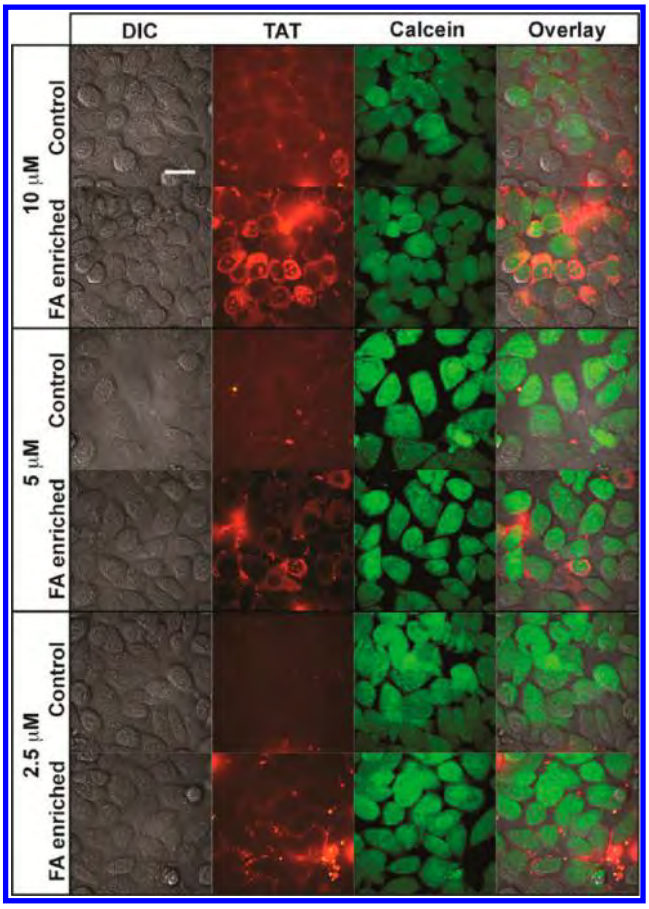

Figure 6. Enriching the plasma membrane with fatty acids enhances the binding and uptake of arginine-rich peptides. To test whether the cellular plasma membrane content of fatty acids can alter the uptake efficiency of RRPs, cells were incubated in a buffer rich in fatty acids for 15 min, washed, and incubated with added RRPs (10, 5, or 2.5 μM) for 5 min keeping the pH at 7.5. The cells were then washed and regular cell culture medium plus calcein was added, and the cells were imaged. In the first column are shown DIC images, in the second column the fluorescence emission of TAMRA-labeled TAT, in the third column the fluorescence intensity of calcein, and in the last column the overlay of the three channels. Scale bar = 25 μm.

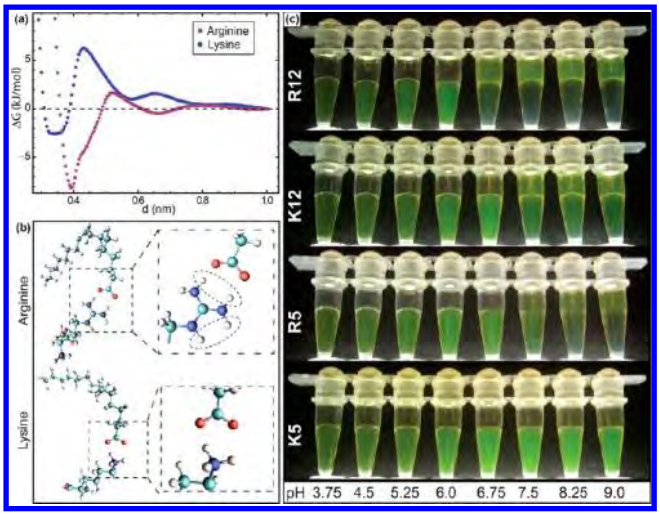

Figure 7. Arginine amino acids have a higher affinity for fatty acids than lysine amino acids. (a) Computed free energy profiles as functions of the distance between the carbon atom of the deprotonated carboxyl acid group (of the oleic acid) and the carbon atom of the guanidium group (arginine amino acid) or the carbon atom of the amino group (lysine amino acid). There is a gain in free energy 4 times higher for the binding of an arginine amino acid to an oleic acid relative to the binding of a lysine amino acid. (b) Snapshots of conformations of the amino acids at the positions where the free energy reaches a minimum, showing a more favorable alignment and hydrogen bonding in the case of the guanidinium group relative to the amino group. (c) Hydrophobic absorption of arginine and lysine amino acids at different pHs and numbers of residues. The photographs show polyarginine and polylysine peptides labeled with FITC in microcentrifuge tubes composed of two phases as described in Figure 1. The absorption into the hydrophobic phase is stronger for polyarginine peptides than for polylysine peptides. There is a sharp transition from the aqueous phase to the octanol phase at pH 6.75 for R12, while in the case of K12 this transition is shifted to a higher pH. Comparing R12 with R5, the absorption into the hydrophobic phase is shifted to a higher pH for R5, while K5 is not absorbed into the hydrophobic phase within this pH range.

Therefore, guanidinium groups bind more easily to fatty acids and in doing so gain significantly more energy. Figure 7b shows snapshots of the conformations of an arginine and a lysine amino acid at the position of the minimum free energy in each case.

Next, we experimentally tested the fatty acid absorption of polyarginine and polylysine peptides of different lengths in the octanol phase. Figure 7c shows experimental images of the partition of polyarginine and polylysine peptides between octanol with 1% oleic acid and aqueous phases at different pHs. We can see that K12 can be partially absorbed into the octanol phase at a higher pH than R12. R5 also partitions in the octanol phase at higher pH than R12, while K5 is unable to partition into the octanol phase within this pH range. Therefore, the interplay between fatty acids and proton density captures the essence of the puzzling observations reported in previous works showing that polylysines or short polyarginine sequences such as R5 are unable to efficiently transduce into living cells.

3. CONCLUSION

Theoretical computations, in vitro and live-cell experiments reveal a mechanism in which fatty acids mediate the absorption and transport of RRPs across a hydrophobic barrier from a high- to a low-pH environment. This mechanism (depicted in Scheme 1) is essentially possible in cells because the intracellular pH in most cells is actively kept near neutral and at this pH plasma membrane fatty acids become protonated, while at a higher pH they become deprotonated. Deprotonated fatty acids in contact with the extracellular medium kept at higher pH bind to guanidinium groups with very high affinity, facilitating the absorption and peptide transport across the hydrophobic core of the plasma membrane nucleating a channel. In contact with the lower cytosolic pH, fatty acids become protonated and neutrally charged, and the RRPs are released from the plasma membrane into the cells and the channel closes. Protonated fatty acids freely diffuse across the plasma membrane, when in contact with the extracellular medium they get deprotonated, becoming negatively charged and trapped in the extracellular layer of the plasma membrane. Then, this cycle can then be repeated.

The possibility that these peptides might be able to directly cross the cell plasma has led, since their discovery, to a search for compounds that could enhance their cellular uptake. The

dx.doi.org/10.1021/ja507790z | J. Am. Chem. Soc. 2014, 136, 17459−17467

Scheme 1. Proposed Cellular Uptake Mechanism for Arginine-Rich Cell-Penetrating Peptides[a]

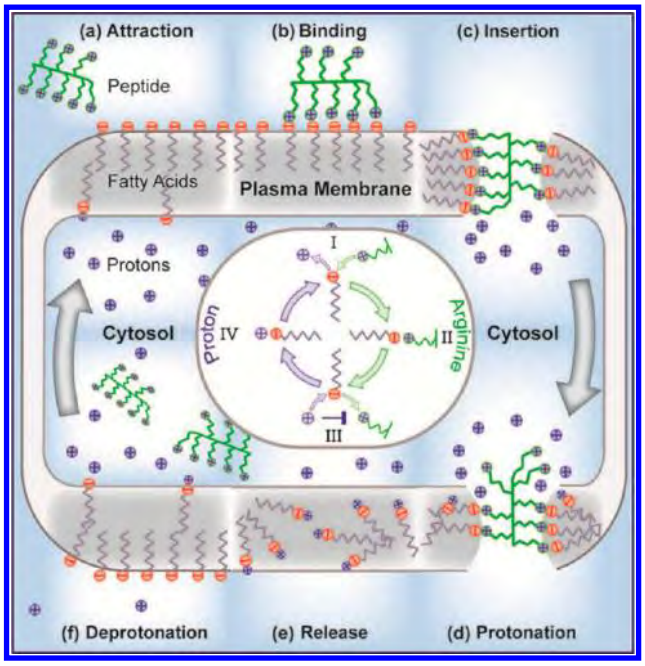

[a](a) The peptide located in the extracellular medium is attracted and (b) binds to deprotonated fatty acids. (c) The peptide–fatty acid complex nucleates a water channel. (d) This peptide–fatty acid complex diffuses across this channel while simultaneously protons from the cytosolic side compete for the binding of the guanidinium groups to fatty acids. (e) The high density of protons in the cytosol protonates the fatty acids, and the peptide gets released into the cytosol. (f) The channel closes, and neutral fatty acids freely diffuse across the plasma membrane; when they come into contact with the extracellular medium, they are deprotonated. The headgroups of the fatty acids become negatively charged and trapped in the extracellular layer of the plasma membrane, and the cycle can repeat again. The inset highlights that essentially fatty acids are able to get inserted into plasma membrane, transporting arginine-rich peptides (or guanidinium-rich molecules) toward the cytosol and protons toward the exterior of the cell. In the cytosol, fatty acids get protonated, inhibiting the binding of fatty acids to guanidinium groups.

mechanism outlined here explains at a fundamental level the enhancement effect of pyrenebutyrate on the cellular uptake of RRPs. The essential ingredients in the mechanism presented here are the guanidinium groups, the carboxyl groups coupled to a hydrophobic moiety, and the pH gradient across the plasma membrane. Accordingly, increasing any of these ingredients leads to a significant increase in transduction efficiency.

The mechanism uncovered by these experiments provides a unifying perspective on the cellular transduction of arginine-rich cell-penetrating peptides. The simplicity and universality of the elements involved in this mechanism elegantly reveals how these peptides are able to efficiently cross in an energy- and receptor-independent manner into virtually any cell type.

■ ASSOCIATED CONTENT

Supporting Information

Experimental and theoretical methods, chemical compounds, supporting figures, and supporting movies (AVI). This material is available free of charge via the Internet at http://pubs.acs.org.

■ AUTHOR INFORMATION

Corresponding Author

angel@rpi.edu

Notes

The authors declare no competing financial interest.

■ ACKNOWLEDGMENTS

This work was funded by National Institutes of Health (Grant GM086801) and the German Research Council (DFG) (Grant CA198/8). This work used the Extreme Science and Engineering Discovery Environment (XSEDE) (request numbers MCB130086 and MCB140075). The authors thank Anne Lehmkuhl for excellent technical assistance, and C. Neale, O. Suarez, B. Barquera and L. Ligon for proofreading the article and excellent discussions.

■ REFERENCES

(1) Frankel, A. D.; Pabo, C. O. *Cell* **1988**, *55*, 1189–1193.
(2) Bechara, C.; Sagan, S. *FEBS Lett.* **2013**, *587*, 1693–1702.
(3) MacEwan, S. R.; Chilkoti, A. *Wiley Interdiscip. Rev.: Nanomed. Nanobiotechnol.* **2013**, *5*, 31–48.
(4) Margus, H.; Padari, K.; Pooga, M. *Mol. Ther.* **2012**, *20*, 525–533.
(5) Walrant, A.; Bechara, C.; Alves, I. D.; Sagan, S. *Nanomedicine* **2012**, *7*, 133–143.
(6) Mussbach, F.; Franke, M.; Zoch, A.; Schaefer, B.; Reissmann, S. *J. Cell. Biochem.* **2011**, *112*, 3824–3833.
(7) Herce, H. D.; Deng, W.; Helma, J.; Leonhardt, H.; Cardoso, M. C. *Nat. Commun.* **2013**, *4*, No. 2660.
(8) Lättig-Tünnemann, G.; Prinz, M.; Hoffmann, D.; Behlke, J.; Palm-Apergi, C.; Morano, I.; Herce, H. D.; Cardoso, M. C. *Nat. Commun.* **2011**, *2*, No. 453.
(9) Tünnemann, G.; Cardoso, M. C. Cell-Penetrating Peptides—Uptake, Toxicity and Applications. In *Membrane-Active Peptides: Methods and Results on Structure and Function*; Castanho, M., Ed.; IUL Publishers: La Jolla, CA, 2009; pp 331–362.
(10) Ter-Avetisyan, G.; Tünnemann, G.; Nowak, D.; Nitschke, M.; Herrmann, A.; Drab, M.; Cardoso, M. C. *J. Biol. Chem.* **2009**, *284*, 3370–3378.
(11) Säälik, P.; Niinep, G.; Pae, J.; Hansen, M.; Lubenets, D.; Langel, Ü.; Pooga, M. *J. Controlled Release* **2011**, *153*, 117–125.
(12) Duchardt, F.; Fotin-Mieczek, M.; Schwarz, H.; Fischer, R.; Brock, R. *Traffic* **2007**, *8*, 848–866.
(13) Jiao, C.-Y.; Delaroche, D.; Burlina, F.; Alves, I. D.; Chassaing, G.; Sagan, S. *J. Biol. Chem.* **2009**, *284*, 33957–33965.
(14) Kaplan, I. M.; Wadia, J. S.; Dowdy, S. F. *J. Controlled Release* **2005**, *102*, 247–253.
(15) Sakai, N.; Matile, S. *J. Am. Chem. Soc.* **2003**, *125*, 14348–14356.
(16) Rothbard, J. B.; Jessop, T. C.; Lewis, R. S.; Murray, B. A.; Wender, P. A. *J. Am. Chem. Soc.* **2004**, *126*, 9506–9507.
(17) Esbjorner, E. K.; Lincoln, P.; Norden, B. *Biochim. Biophys. Acta* **2007**, *1768*, 1550–1558.
(18) Herce, H. D.; Garcia, A. E. *Proc. Natl. Acad. Sci. U.S.A.* **2007**, *104*, 20805–20810.
(19) Herce, H. D.; Garcia, A. E. *J. Biol. Phys.* **2007**, *33*, 345–356.
(20) Herce, H. D.; Garcia, A. E.; Litt, J.; Kane, R. S.; Martin, P.; Enrique, N.; Rebolledo, A.; Milesi, V. *Biophys. J.* **2009**, *97*, 1917–1925.
(21) Ciobanasu, C.; Siebrasse, J. P.; Kubitscheck, U. *Biophys. J.* **2010**, *99*, 153–162.
(22) Piantavigna, S.; McCubbin, G. A.; Boehnke, S.; Graham, B.; Spiccia, L.; Martin, L. L. *Biochim. Biophys. Acta* **2011**, *1808*, 1811–1817.
(23) Bouchet, A. M.; Lairion, F.; Ruysschaert, J.-M.; Lensink, M. F. *Chem. Phys. Lipids* **2012**, *165*, 89–96.
(24) Boll, A.; Jatho, A.; Czudnochowski, N.; Geyer, M.; Steinem, C. *Biochim. Biophys. Acta* **2011**, *1808*, 2685–2693.
(25) Choi, D.; Moon, J. H.; Kim, H.; Sung, B. J.; Kim, M. W.; Tae, J. Y.; Satija, S. K.; Akgun, B.; Yu, C.-J.; Lee, H. W.; Lee, D. R.;

Henderson, J. M.; Kwong, J. W.; Lam, K. L.; Lee, K. Y. C.; Shin, K. *Soft Matter* **2012**, *8*, 8294−8297.
(26) Chen, X.; Sa'adedin, F.; Deme, B.; Rao, P.; Bradshaw, J. *Biochim. Biophys. Acta* **2013**, *1828*, 1982−1988.
(27) Mishra, A.; Gordon, V. D.; Yang, L.; Coridan, R.; Wong, G. C. L. *Angew. Chem., Int. Ed.* **2008**, *47*, 2986−2989.
(28) Kanicky, J. R.; Shah, D. O. *J. Colloid Interface Sci.* **2002**, *256*, 201−207.
(29) Salentinig, S.; Sagalowicz, L.; Glatter, O. *Langmuir* **2010**, *26*, 11670−11679.
(30) Harms, M. J.; Schlessman, J. L.; Sue, G. R.; Garcia-Moreno E., B. *Proc. Natl. Acad. Sci. U.S.A.* **2011**, *108*, 18954−18959.
(31) Katayama, S.; Nakase, I.; Yano, Y.; Murayama, T.; Nakata, Y.; Matsuzaki, K.; Futaki, S. *Biochim. Biophys. Acta* **2013**, *1828*, 2134−2142.
(32) Guterstam, P.; Madani, F.; Hirose, H.; Takeuchi, T.; Futaki, S.; EL Andaloussi, S.; Gräslund, A.; Langel, Ü. *Biochim. Biophys. Acta* **2009**, *1788*, 2509−2517.
(33) Hatzakis, E.; Koidis, A.; Boskou, D.; Dais, P. *J. Agric. Food Chem.* **2008**, *56*, 6232−6240.
(34) Torrie, G. M.; Valleau, J. P. *J. Comput. Phys.* **1977**, *23*, 187−199.
(35) Herce, D. H.; Perera, L.; Darden, T. A.; Sagui, C. *J. Chem. Phys.* **2005**, *122*, No. 024513.
(36) Huang, K.; Garcia, A. E. *Biophys. J.* **2013**, *104*, 412−420.
(37) Henriques, S. T.; Costa, H.; Castanho, M. A. R. B. *Biochemistry* **2005**, *44*, 10189−10198.
(38) Tünnemann, G.; Martin, R. M.; Haupt, S.; Patsch, C.; Edenhofer, F.; Cardoso, M. C. *FASEB J.* **2006**, *20*, 1775−1784.
(39) Stanzl, E. G.; Trantow, B. M.; Vargas, J. R.; Wender, P. A. *Acc. Chem. Res.* **2013**, *46*, 2944−2954.
(40) Derossi, D.; Calvet, S.; Trembleau, A.; Brunissen, A.; Chassaing, G.; Prochiantz, A. *J. Biol. Chem.* **1996**, *271*, 18188−18193.
(41) Tünnemann, G.; Ter-Avetisyan, G.; Martin, R. M.; Stöckl, M.; Hermann, A.; Cardoso, M. C. *J. Pept. Sci.* **2008**, *14*, 469−476.
(42) Herce, H. D.; Rajan, M.; Lättig-Tünnemann, G.; Fillies, M.; Cardoso, M. C. *Nucleus* **2014**, DOI: 10.4161/nucl.36290.
(43) Futaki, S.; Suzuki, T.; Ohashi, W.; Yagami, T.; Tanaka, S.; Ueda, K.; Sugiura, Y. *J. Biol. Chem.* **2001**, *276*, 5836−5840.
(44) Martin, P.; Moncada, M.; Enrique, N.; Asuaje, A.; Capuccino, J. M. V.; Gonzalez, C.; Milesi, V. *Pflügers Arch.* **2014**, *466*, 1779−1792.
(45) Schroit, A. J.; Gallily, R. *Immunology* **1979**, *36*, 199−205.
(46) Wender, P. A.; Mitchell, D. J.; Pattabiraman, K.; Pelkey, E. T.; Steinman, L.; Rothbard, J. B. *Proc. Natl. Acad. Sci. U.S.A.* **2000**, *97*, 13003−13008.

■ NOTE ADDED AFTER ASAP PUBLICATION

Figure 2 was corrected on December 2, 2014.

Fundamental molecular mechanism for the cellular uptake of guanidinium-rich molecules

Supplementary Information

Henry D. Herce[1], Angel E. Garcia[1,†], and M. Cristina Cardoso[2]

Materials and methods

Peptides: 5-carboxytetramethylrhodamine (TAMRA)-TAT (GRKKRRQRRR) peptides were synthesized as D-isomers and coupled directly to TAMRA at the N terminus, while R5, R8, R12, K5, K10 and K12 were synthesized as L-isomers and coupled directly to fluorescein-isothiocyanate (FITC) at the N terminus (Peptide Specialty Laboratories GmbH, Heidelberg, Germany). R10 peptides were synthesized as D-isomers and coupled directly to fluorescein-isothiocyanate (FITC) at the N terminus while the cR10 peptides were synthesized intercalating L- and D-isomers as described in [1]. TATssPL* was synthesized by Biosyntan GmbH (Berlin, Germany).

Table 1. Summary of peptides. The fluorophores 5-carboxytetramethylrhodamine (TAMRA) and fluorescein-isothiocyanate (FITC) were used for labeling the peptides. L amino acids are spelled using a capital letters while D amino acids are not capitalized and (-CC-) refers to a disulfide bridge.

Name	Sequence
TAT	**TAMRA**-rrrqrrkkrg
R5	**FITC**-RRRRR
R6	**FITC**-RRRRRR
R8	**FITC**-RRRRRRRR
R10	**FITC**-rrrrrrrrrr
R12	**FITC**-RRRRRRRRRRRR
cR10	**FITC**-KrRrRrRrRrRE- (cyclic)
K5	**FITC**-KKKKK
K10	**FITC**-KKKKKKKKKK
K12	**FITC**-KKKKKKKKKKKK
TATssPL*	RRRQRRKKRG-CC-SAVLQKKITKYFHPKKG-EDA-**TAMRA**

Reagents: Olive oil was purchased from Oliveira da Serra, product name "1ª Colheita" (Figueira dos Cavaleiros, Portugal). Refined Castor oil from Caesar & Loretz GmbH (Hilden, Germany) was purchased from Kronen Pharmacy (Darmstadt, Germany). Octanol, oleic acid and other reagents were purchased from Sigma Aldrich and used without further purification.

Buffers: All buffers used for peptide studies were prepared with 140 mM NaCl, 2.5 mM KCl, 5 mM HEPES, 5 mM glycine, and the pH was adjusted with NaOH or HCl.

Peptides absorption into a hydrophobic phase as a function of pH: Peptides were diluted to a final concentration of 10 μM at each pH. Equal volumes of the buffer-peptide mix at each pH and of octanol plus 1 % of oleic acid were placed into individual microcentrifuge tubes (as shown if Figure 1 (a)). Each pH mix was vortexed for 5 min and centrifuged for 2 min with a centripetal force of 2200 g to quickly separate the octanol from the aqueous phase. Although the fraction of peptides absorbed into the octanol phase could be inferred from the fraction left into the aqueous phase we extracted it from the octanol phase and measure it. To measure directly the relative concentration of peptide absorbed in the octanol phase we used the fact that no peptide absorption into the octanol phase was detected at pH 4. Therefore, the octanol phase was extracted with a pipette and mixed with a buffer at pH 4 separately for each pH into microcentrifuge tubes, which were also vortexed and centrifuged. In this way the fraction of peptide previously absorbed in the octanol phase for each pH was reabsorbed in a pH 4 buffer and now the octanol phase with little or no traces of the TAT peptides was again removed with a pipette and discarded. The peptide in each buffer solution was measured using a fluorescent spectrometer, using as a reference a buffer solution of 10 μM peptide at pH 4, measuring the relative fluorescent intensity emission between the reference solution and the solution of interest, exciting with a laser wavelength of 543 nm and measuring the emission wavelength of 575 nm. Similarly the peptides that remained in the aqueous phase were compared to a reference solution of 10 μM peptide at each pH without having been in contact with the octanol phase.

The protocol for the control experiment to determine the behavior of the TAMRA dye with pH (Figure S1) was done analogously. In this case to extract and directly measure the relative fluorescence intensity of the dye absorbed in the octanol phase, it was used a buffer at pH 9 to reabsorbe the dye previously absorved into the octanol phase (at low pH in this case).

Peptide translocation across a hydrophobic phase from high to low pH: As described in Figure 3 (a), two separate compartments contained in a bigger compartment were built by

cutting the top of two 0.5 ml microcentrifuge tubes and inserting them into a polypropylene BD falcon round-bottom tube. The top of the falcon tube was cut leaving 2 cm from the bottom. One of the interior tubes was filled with 200 μl of the buffer at pH 7.5 plus the peptide and the other interior tube was filled with a buffer at pH 4. Before adding the octanol/oleic acid mix, the space between the two compartments and the falcon tube was filled with glycerol to reduce the amount of octanol solution required to connect the high and low pH chambers. This step was important to reduce the hydrophobic volume accessible to the peptide and speed up the peptide translocation. On top was added a solution 400 μl of octanol plus 1 % of oleic acid previously vortexed and each one was closed with a cap to avoid evaporation. Five of these experimental setups were built for each experiment repetition. One was left untouched for photographic imaging and each one of the others were dismantled every 2 hours, by removing and discarding the octanol phase and measuring the relative fluorescence of each compartment using a fluorescence spectrometer, exciting with a laser wavelength of 543 nm and measuring the emission wavelength of 575 nm.

Cells and Culture Conditions: Human cell lines HeLa and HepG2 were cultured in Dulbecco's modified eagle medium (DMEM) supplemented with 10 % fetal calf serum, 50 μg/ml gentamicin and 2mM glutamine. Mouse myoblasts C2C12 [2] cells were cultured in DMEM supplemented with 20 % fetal calf serum, 50 μg /ml gentamicin and 2mM glutamine. Mouse fibroblasts Flp 3T3 was grown in similar conditions but supplemented only with 10 % FCS. Baby hamster kidney (BHK) cell line was grown in Glasgow minimal essential medium supplemented with 10 % fetal calf serum, 50 μg/ml gentamicin, 2 mM glutamine and 150 μg/ml hygromycin B [3]. All mammalian the cell lines were grown at 37° C in a humidified atmosphere with 5 % CO_2. Insect cells, from Spodoptera frugiperda pupal ovarian tissue (SF9) were cultured in Ex-Cell 420 media supplemented with 10 % FCS, without CO_2 at a 27° C, in suspension cultures shaked permanently at 105 rpm. Bright yellow (BY-2) tobacco cells [4] were grown in suspension in the dark at 25 °C on a rotary shaker (115 rpm) in modified Murashige-Skoog basal medium, supplemented with 1.5 mM KH2PO4, 3 mM thiamine, 0.55 mM inositol, 87 mM Suc, and 1mM 2,4-dichlorophenoxy acetic acid. Media components were purchased from Sigma-Aldrich, Steinheim, Germany.

Confocal Microscopy: Confocal images were collected using an Ultra VIEW VoX spinning disc system (Perkin Elmer) on a Nikon Ti microscope equipped with an oil immersion Plan Apochromat VC ×60/1.45 NA (pixel size in XY = 111 nm, Z-step = 0.3–1 μm), a non-immersion Plan Apochromat VC ×20/0.75 NA and a Plan Fluor 20XMI/0.75 NA multi-immersion objective

lenses, with laser lines at 488 nm, 561 nm, a differential interference contrast (DIC) setup, and a temperature, humidity and CO_2 incubation control (ACU control, Olympus).

TAT cellular uptake in HeLa cells: Cells where seeded at 60 % confluence in a tissue culture treated 6 channel µ-Slide VI (from Ibidi GmbH, Germany) 24 hours before peptide treatment. The uptake imaging at different pHs was done by washing two times with the HEPES buffers at the pH of interest and replacing the buffer solution with the HEPES buffer with the peptide added at a final concentration of 2 µM. The sample was taken to the microscope and imaged at equally spaced intervals of 2 min. This was done simultaneously for pH 6, 7.5 and 9 to compare the relative peptide uptake side by side. HeLa cells were imaged by swapping at each time point between two objectives, a x60 and a x20 immersion oil. This was done to be able to perform two types of time-lapse analysis over the same sample to compute the cellular uptake of the TAT peptide. With the x20 objective is possible to simultaneously visualize several cells but is not easy to separate the fluorescence intensity from internalized peptide from the fluorescent intensity of membrane bound peptide. With the x60 objective a fewer number of cells are visualized but the relative intensity of free peptide can be computed by measuring the fluorescence intensity of peptides accumulated at the nucleolus, since peptide bound to the cell plasma membrane or trapped in endosomes cannot reach the nucleolus [1]. Using the x20 images, the uptake was computed by measuring the average background fluorescence intensity in an area of the images without cells and subtracting this value from the average intensity of the whole image. Using the x60 images, the uptake was computed by measuring the average background fluorescence intensity in an area without cells and subtracting this value from the average intensity in the nucleus. The nucleus area was obtained using the DIC channel. This experiment was repeated 3 times and the average and the standard error plotted. In each experiment, after 30 min the cells were washed with DMEM cell culture media and calcein was added to detect cell viability at a final concentration of 5 µM. In live cells, the non-fluorescent calcein AM is converted to green-fluorescent calcein, after acetoxymethyl ester hydrolysis by intracellular esterases. This was incubated for 30 min and then imaged. Cell viability was also assessed using the DIC images used to detect the cell morphology along the experiments. To further evaluate the viability of cells after uptake of the TAT at pH 9, cell division was monitored for 16 hours.

TAT cellular uptake in different species and kingdoms: The cellular uptake in the rest of the cell lines was monitored with a single objective through each experiment (either a x20 or a x60). The TAT peptide concentration in each cell line uptake experiment was adjusted to obtain

peptide uptake in more than 60 % of the cells at pH 9 within 30 min. Peptide uptake was monitored simultaneously for pH 6, 7.5 and 9 to compare the relative peptide uptake side by side. Experiments were repeated 3 times for each cell line and at least 300 cells. The proportion of cells displaying uptake was visually counted and the average and standard error values computed.

Cellular uptake in fatty acid enriched cells: A HEPES buffer at pH 7.5 was mixed with 0.2 % volume of oleic acid. Cells were washed twice and incubated for 15 min with this buffer. Next, cells were washed once with a HEPES buffer at pH 7.5 (without oleic acid) and the TAT peptide mixed with this last buffer was added at different concentrations. Cells were washed after 5 min with DMEM cell culture media two times and imaged. This was followed by the calcein viability test as described previously.

Umbrella sampling computation of TAT free energy insertion into model bilayers: Molecular dynamics simulations were performed to study the translocation energetics of the protein transduction domain of the HIV-1 TAT across model membranes, the TAT peptide water-octanol/fatty acid partition, and the energetics of arginine and lysine interactions with deprotonated fatty acids [5-7].

The free energy of insertion of a TAT peptide into model lipid membranes was measured by placing the TAT peptide in a periodically repeating box containing a pre-equilibrated lipid bilayer composed of 64 1,2-Dioleoyl-sn-Glycero-3-Phosphocholine (DOPC) lipids, 48 oleic acids (protonated and/or deprotonated), neutralizing potassium counter ions and 8700 water molecules. In different umbrella sampling calculations the TAT peptide was placed at 31 windows separated by 0.075 nm intervals from the center of mas of the bilayer in a direction perpendicular to the bilayer plane. The center of mass of each peptide was restraint by a harmonic potential at each position with a force constant of 3000 kJ/(mol nm^2). The weighted histogram analysis method (WHAM) was used to compute the free energy of insertion of the peptide along this path.[8] Each independent simulation was equilibrated for at least 300 ns and the data collection was done over an extra 40 ns. The total computed time for each free energy calculation expanded 10.2 μs. Free energy block averages of 4 ns was computed over the last 100 ns to obtain the standard deviation.

Molecular dynamics computation of TAT partition into water/octanol phases: The partition of the TAT peptide into the water/octanol phases was studied by mixing 4 TAT peptides, 64 oleic acids (all protonated or all deprotonated), 16000 octanol molecules, 24000 water

molecules and counter ions to neutralize the systems (chloride or potassium respectively). Experimentally, the octanol and water phases separate into to two bulk phases by the effect of the gravitational force, the less dense octanol o top of the denser water phase. The same effect is produced by a centripetal force. Therefore, we modeled a centripetal force by adding an external force in the z direction over each atom given by $F=k\ m\ (z-L_z/2)$, with m being the mass of each atom, $k=0.01\ kJ/(mol\ nm^2)$, and L_z the dimension of the system box in the direction z. Each system was simulated for 300 ns.

Computation of free energy differences between lysine and arginine amino acids: The free energy of interaction profile as a function of the distance between an oleic acid and an arginine (or lysine) amino acid was calculated in systems composed of a single arginine (or lysine) amino acid a single oleic acid, and 2200 water molecules. The distance was restraint using a harmonic potential with a force constant of 3000 $kJ/(mol\ nm^2)$ at 30 positions separated by 0.025 nm, staring from a distance of 0.2 nm, between the first carbon atom of the oleic acid and the central carbon of the guanidinium group (or nitrogen of the amino group). The weighted histogram analysis method (WHAM) was used to compute the free energy of insertion of the peptide along this path.[9] Each independent simulation was equilibrated for at least 30 ns and the data collection was done over an extra 30 ns. The total computed time for each free energy calculation expanded at least 1.8 μs.

Molecular dynamics software and parameters: The simulations were performed using the GROMACS package, version 4.5.6 [10, 11]. The overall temperature of the water, lipids, and peptides was kept constant, coupling independently each group of molecules at 323 K with a v-rescale thermostat. The pressure was coupled to a Berendsen barostat at 1 atm separately in the direction perpendicular to the bilayer plane and in the directions parallel to the bilayer. The temperature and pressure time constants of the coupling were 0.2 and 2 ps, respectively. The integration of the equations of motion was performed by using a leap frog algorithm with a time step of 2 fs. Periodic boundary conditions were implemented in all systems. A cutoff of 1 nm was implemented for the Lennard–Jones and the direct space part of the Ewald sum for Coulombic interactions. The Fourier space part of the Ewald splitting was computed by using the particle-mesh Ewald method [12], with a grid length of 0.11 nm on the side and a cubic spline interpolation. We used the CHARMM TIP3P [13] water model, for the lipids and peptides it was used the force field CHARMM 36.

1. Lattig-Tunnemann, G., et al., *Backbone rigidity and static presentation of guanidinium groups increases cellular uptake of arginine-rich cell-penetrating peptides.* Nat Commun, 2011. **2**: p. 453.

2. Yaffe, D. and O. Saxel, *Serial passaging and differentiation of myogenic cells isolated from dystrophic mouse muscle.* Nature, 1977. **270**(5639): p. 725-727.

3. Tsukamoto, T., et al., *Visualization of gene activity in living cells.* Nat Cell Biol, 2000. **2**(12): p. 871-8.

4. Nagata, T., Y. Nemoto, and S. Hasezawa, *Tobacco by-2 Cell-Line as the Hela-Cell in the Cell Biology of Higher-Plants.* International Review of Cytology-a Survey of Cell Biology, 1992. **132**: p. 1-30.

5. Feller, S.E., et al., *Molecular dynamics simulation of unsaturated lipid bilayers at low hydration: parameterization and comparison with diffraction studies.* Biophys J, 1997. **73**(5): p. 2269-79.

6. Klauda, J.B., et al., *Update of the CHARMM all-atom additive force field for lipids: validation on six lipid types.* J Phys Chem B, 2010. **114**(23): p. 7830-43.

7. Klauda, J.B., et al., *Improving the CHARMM force field for polyunsaturated fatty acid chains.* J Phys Chem B, 2012. **116**(31): p. 9424-31.

8. Kumar, S., et al., *The Weighted Histogram Analysis Method for Free-Energy Calculations on Biomolecules .1. The Method.* Journal of Computational Chemistry, 1992. **13**(8): p. 1011-1021.

9. Torrie, G.M. and J.P. Valleau, *Nonphysical sampling distributions in Monte Carlo free-energy estimation: Umbrella sampling.* Journal of Computational Physics, 1977. **23**(2): p. 187-199.

10. Van Der Spoel, D., et al., *GROMACS: fast, flexible, and free.* Journal of Computational Chemistry, 2005. **26**(16): p. 1701-18.

11. Pronk, S., et al., *GROMACS 4.5: a high-throughput and highly parallel open source molecular simulation toolkit.* Bioinformatics, 2013. **29**(7): p. 845-54.

12. Darden, T., D. York, and L. Pedersen, *Particle Mesh Ewald - an N.Log(N) Method for Ewald Sums in Large Systems.* Journal of Chemical Physics, 1993. **98**(12): p. 10089-10092.

13. MacKerell, A.D., et al., *All-atom empirical potential for molecular modeling and dynamics studies of proteins.* Journal of Physical Chemistry B, 1998. **102**(18): p. 3586-3616.

Supplementary Figures

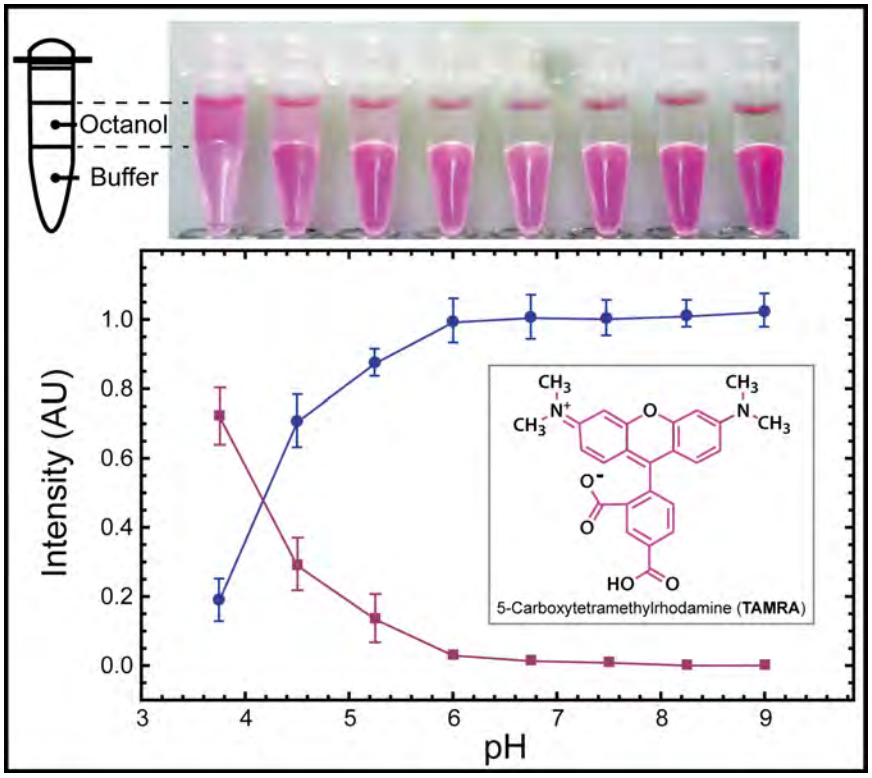

Figure S1. Arginine-rich peptides drive the fluorescent dyes used in this study towards the aqueous or octanol phase. TAMRA (5-Carboxytetramethylrhodamine) and FITC (Fluorescein isothiocyanate**)** fluorescent dyes get protonated as the pH is lowered becoming more hydrophobic and prompt to partition into the hydrophobic phase. This is the opposite behavior as when they are coupled to arginine- and lysine-rich peptides (Figure 1, 2, 3 and 7) indicating that the peptides drive the partition of the dyes into the aqueous phase at low pH and into the hydrophobic phase at high pH. While the partition fluorescein dyes has already been reported (Oba, Y et al. Geochem J, 2012. **46**: p. 517-20), to our knowledge, there is no study on the partition of TAMRA. Therefore, as a control experiment, here we studied the partition of TAMRA following the same protocol as in Figure 1 (a). The photograph and the plot show that for a pH less than 6 TAMRA (10 μM) partitions partially into the octanol phase, while for any larger pH partitions exclusively in the aqueous phase. This partitioning is essentially determined by the protonation state of the carboxyl acid groups (pKa <5), as these groups become protonated at low pH the fluorescent dyes partition into the hydrophobic phase.

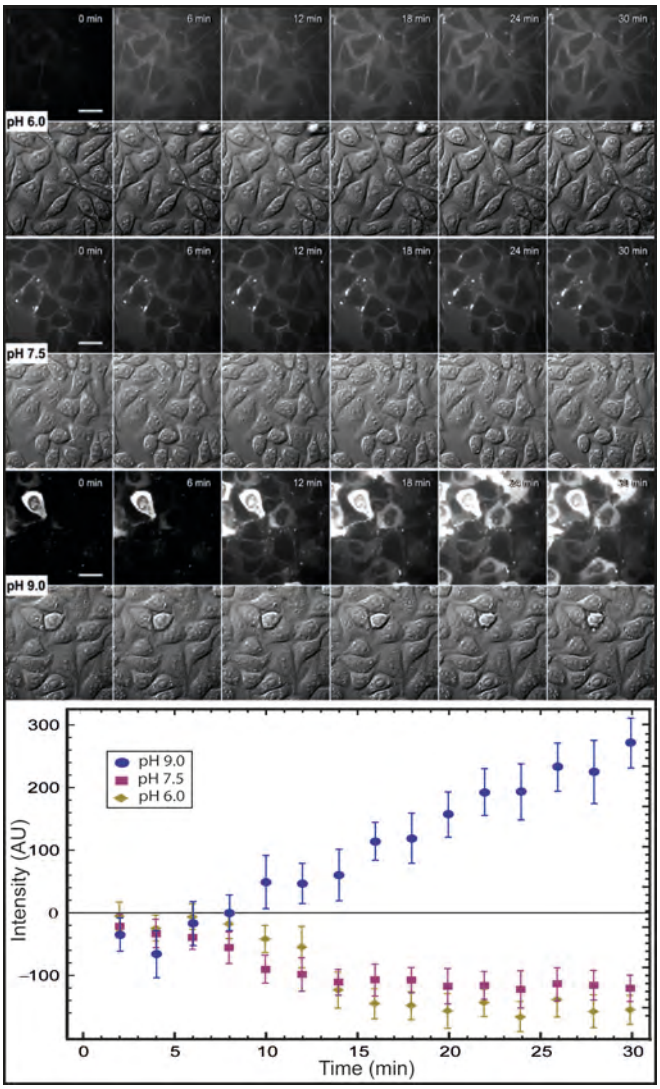

Figure S2 Increasing the extracellular pH consistently increases the transduction efficiency of arginine rich peptides. Time-lapse fluorescence images show the TAT (2 μM) uptake in living cells at pH 6, 7.5 and 9. The lower plot shows the average (over three independent repetitions) of the overall fluorescence intensity minus the background intensity, and standard error of the mean, as a function of time. After 30 min the fluorescence increases several folds at pH 9 relative to pH 6 and pH 7.5. The images where acquired with x60 objective magnification, to quantify only free intracellular distributed peptide, and it was measured over time the fluorescence intensity at the nucleolus relative to the background. Scale bar 15 μm.

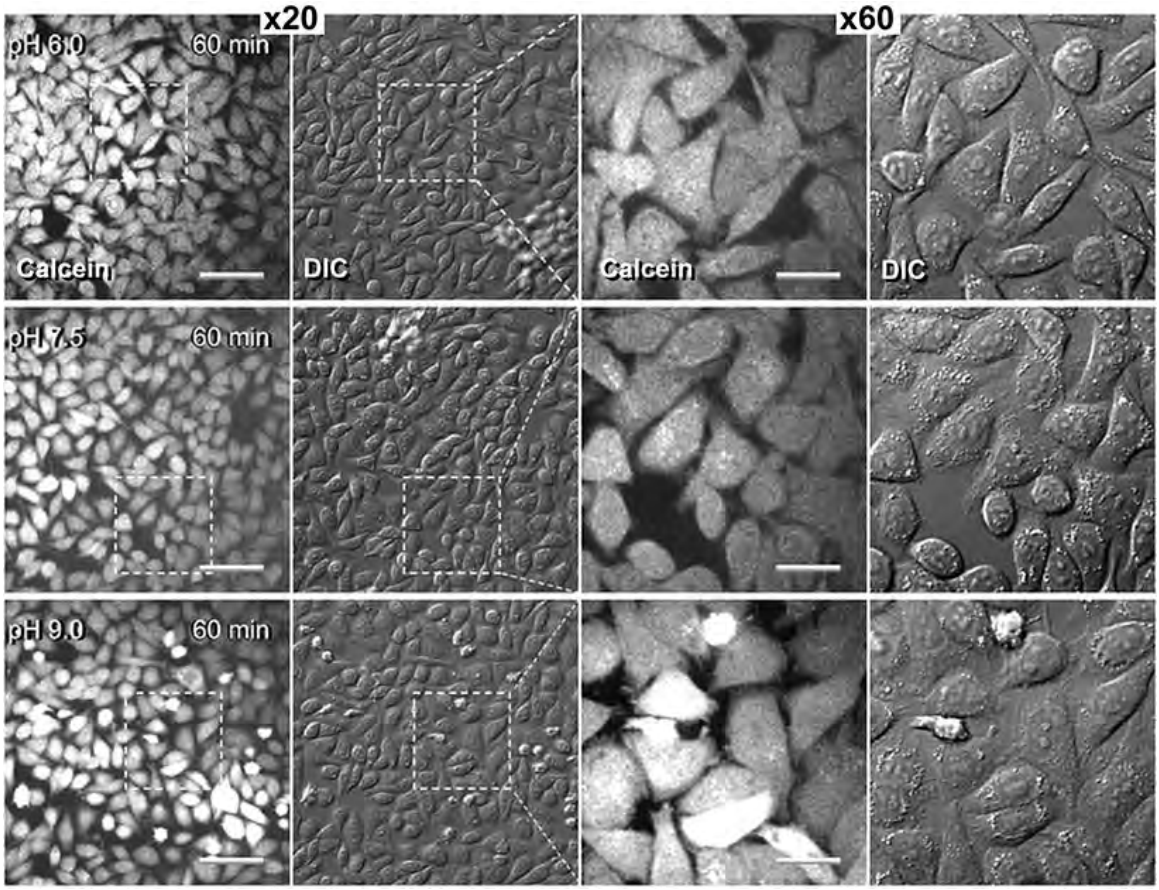

Figure S3. Cells display enzymatic activity after being exposed for 30 min to buffers at pH 6, 7.5 and 9, containing the TAT peptide. After imaging HeLa cells in Figure 4 and Extended Data Figure 2, cells were incubated for an extra 30 min in standard culture media containing calcein AM and imaged again. Calcein AM is a common cell-permeant dye used to determine cell viability in most eukaryotic cells. In live cells the non-fluorescent calcein AM is converted to a green-fluorescent calcein after acetoxymethyl ester hydrolysis by intracellular esterases. Images were acquired using a x20 objective (scale bar 75 μm) and the insets were acquired using a x60 objective (scale bar 15 μm).

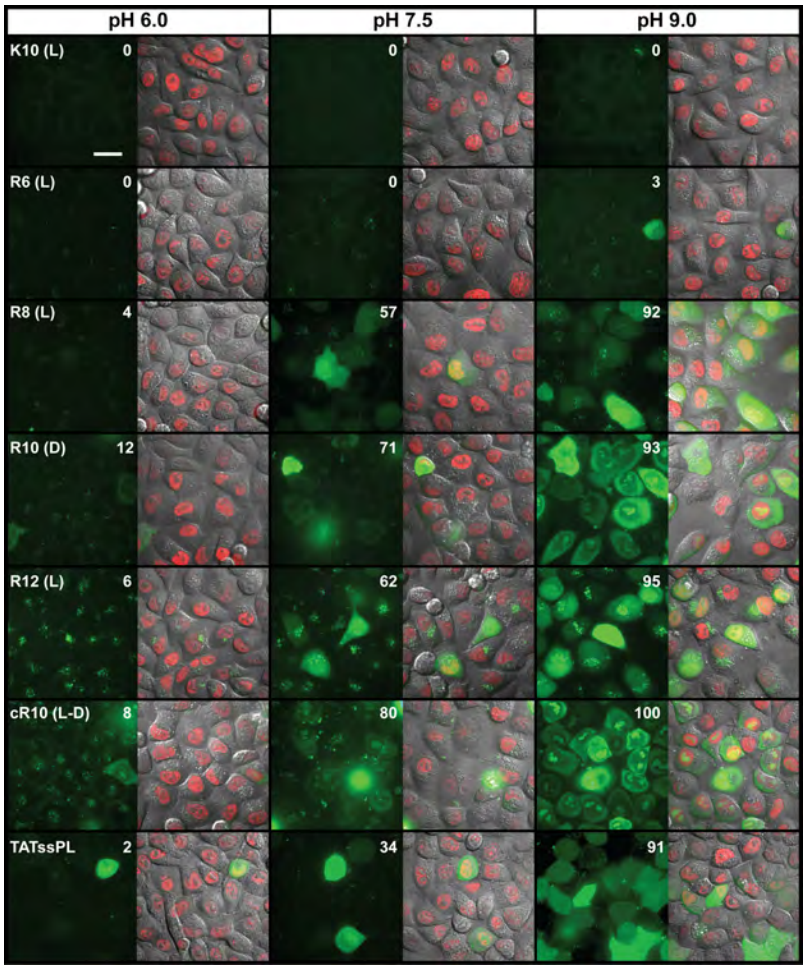

Figure S4. Increasing the extracellular pH consistently increases the transduction efficiency of arginine rich peptides with different structures, lengths and chirality. Fluorescence images show the uptake of the peptides listed in Table 1 (2 μM) in living cells (HeLa) at pH 6, 7.5 and 9 after 30 min. For each pH is shown the fluorescent confocal image of the peptides (green) and an image composed of an overlay of the DIC, the peptides and the nucleus (red). Cells permanently expressing Proliferating Cell Nuclear Antigen (PCNA) labeled with Cherry or GFP were used to facilitate the detection and visualization of confocal planes across the nucleus. This helped to easily classify and count cells containing transduced peptides from the cells that only contain membrane bound peptides. Although, this is clear when the peptides are in D form (R10 or cR10) since they are stable and distinctly label the nucleolus, the peptides in L form are being actively degraded and the signal quickly redistributes more homogeneously within the cell making more challenging to distinguish membrane bound peptides form internalized peptides. Cells were counted as positive when the peptide signal colocalized with the PCNA signal. The percentage of cells counted with intracellular peptide at pH 9 was consistently larger relative to pH 6 and 7.5 for all arginine rich peptides, while the poly-lysine peptide K10 displays no uptake at all pHs The uptake efficiency also increases with the number of arginine amino acids and by cyclization. The images where acquired with a x60 objective magnification. Each experiment was repeated 3 times and the percentage represents the average over more than 400 cells in each case. Scale bar 15 μm.

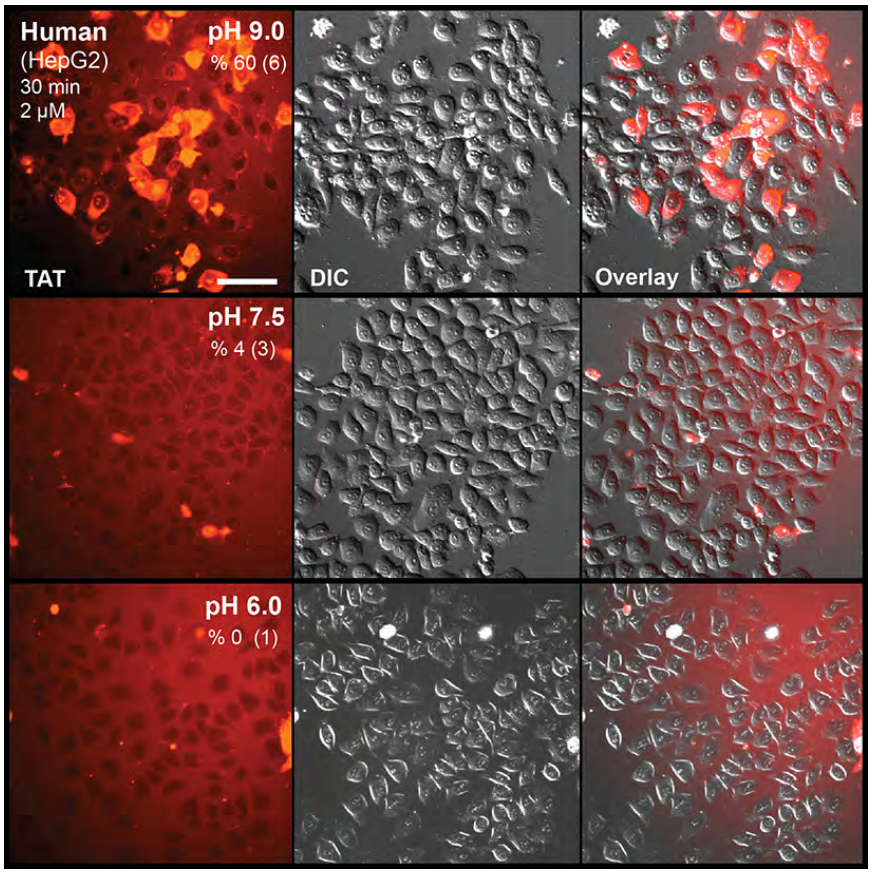

Figure S5. Cellular uptake of the TAT peptide in HepG2 (human liver hepatocellular) cells at ph 6, 7.5 and 9. Live cell confocal microscopy images obtained after 30 min incubation with the TAT peptide (2 μM). In the first column are shown fluorescence images of the TAT peptide labeled with TAMRA indicating the percentage of cells counted with internalized peptide over 3 independent experiments for each pH (standard deviations are shown between parenthesis). In the second column are shown DIC images and in the third column is shown the overlay of the first two columns. Scale bar 75 μm.

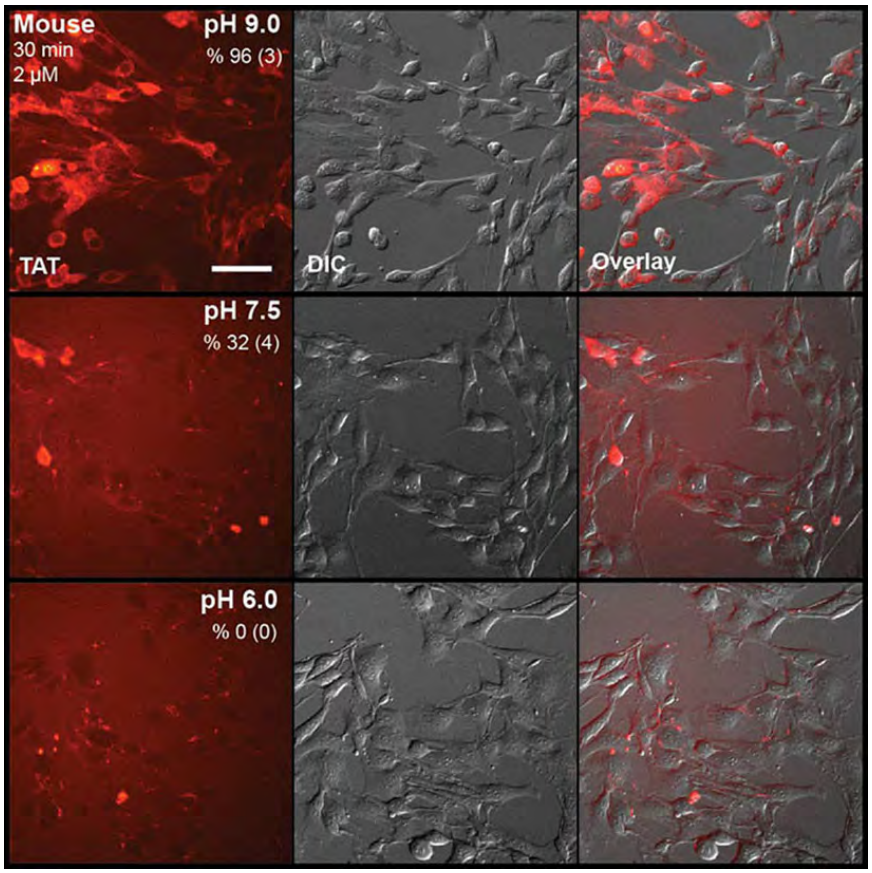

Figure S6 Cellular uptake of the TAT peptide in C2C12 (mouse myoblast) cells at pH 6, 7.5 and 9. Live cell confocal microscopy images obtained after 30 min incubation with the TAT peptide (2 μM). In the first column are shown fluorescence images of the TAT peptide labeled with TAMRA indicating the percentage of cells counted with internalized peptide over 3 independent experiments for each pH (standard deviations are shown between parenthesis). In the second column are shown DIC images and in the third column is shown the overlay of the first two columns. Scale bar 75 μm.

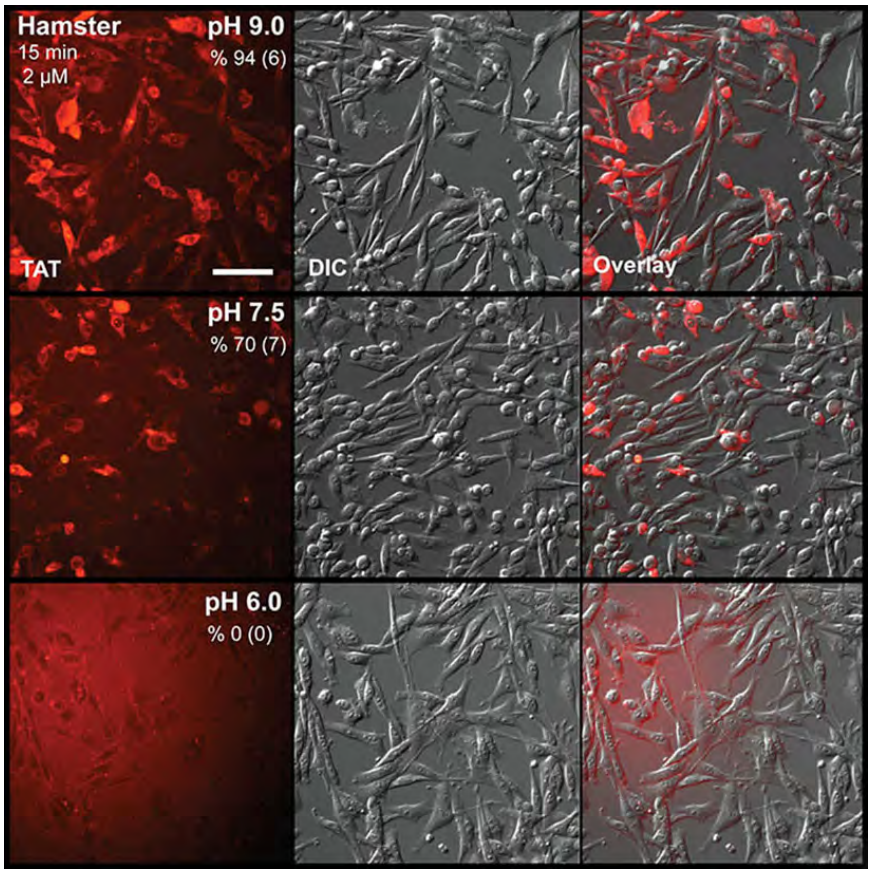

Figure S7 Cellular uptake of the TAT peptide in BHK (baby hamster kidney fibroblasts) cells at pH 6, 7.5 and 9. Live cell confocal microscopy images obtained after 15 min incubation with the TAT peptide (2 μM). In the first column are shown fluorescence images of the TAT peptide labeled with TAMRA indicating the percentage of cells counted with internalized peptide over 3 independent experiments for each pH (standard deviations are shown between parenthesis). In the second column are shown DIC images and in the third column is shown the overlay of the first two columns. Scale bar 75 μm.

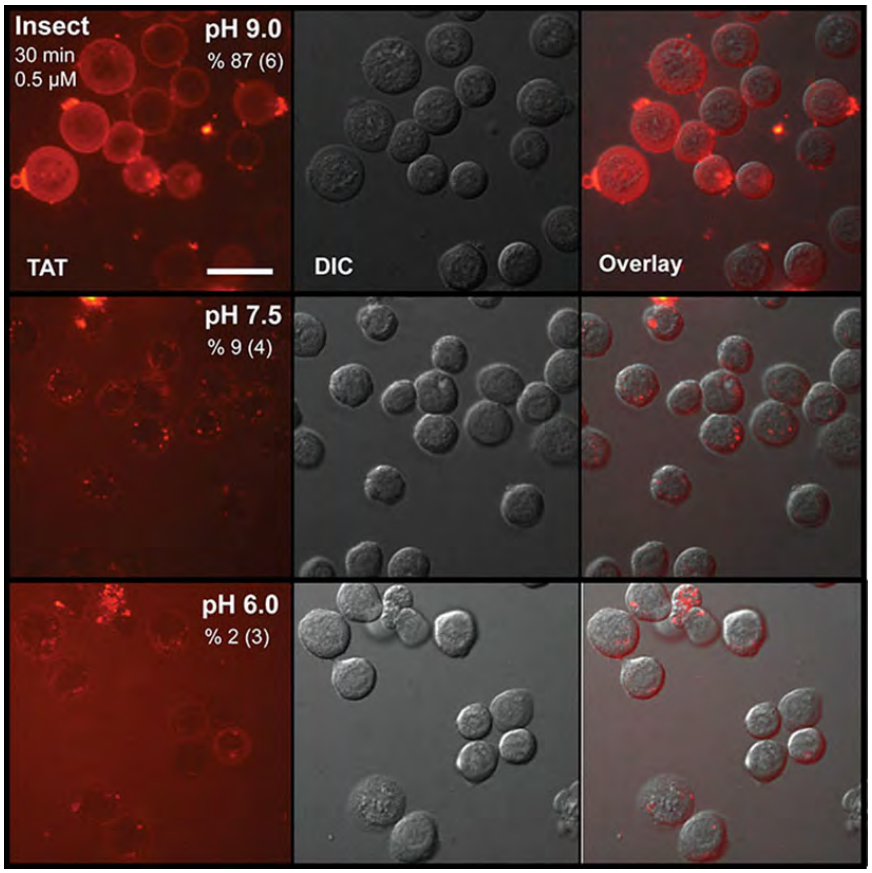

Figure S8 Cellular uptake of the TAT peptide in Sf9 (Spodoptera frugiperda pupal ovarian) cells at pH 6, 7.5 and 9. Live cell confocal microscopy images obtained after 30 min incubation with the TAT peptide (0.5 μM). In the first column are shown fluorescence images of the TAT peptide labeled with TAMRA indicating the percentage of cells counted with internalized peptide over 3 independent experiments for each pH (standard deviations are shown between parenthesis). In the second column are shown DIC images and in the third column is shown the overlay of the first two columns. Scale bar 15 μm.

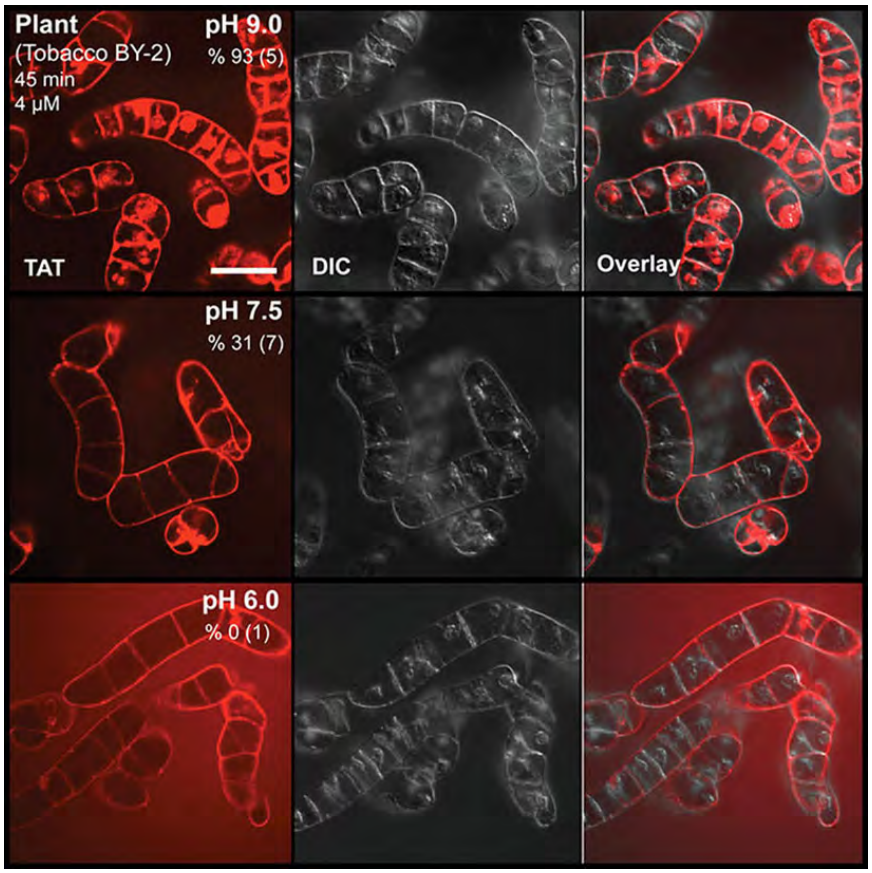

Figure S9 Cellular uptake of the TAT peptide in tobacco plant BY-2 cells at pH 6, 7.5 and 9. Live cell confocal microscopy images obtained after 45 min incubation with the TAT peptide (4 μM). In the first column are shown fluorescence images of the TAT peptide labeled with TAMRA indicating the percentage of cells counted with internalized peptide over 3 independent experiments for each pH (standard deviations are shown between parenthesis). In the second column are shown DIC images and in the third column is shown the overlay of the first two columns. Scale bar 75 μm.

Movie Legends

Movie S1. Structures and free energy computation of the TAT peptide insertion into a phospholipid bilayer containing deprotonated fatty acids using molecular dynamics simulations. In the upper panel are shown molecular conformations of the systems with the peptide constrained along the direction perpendicular to the bilayer. The systems are composed of a TAT peptide, 8700 water molecules, 68 DOPC, 48 oleic acid molecules (all protonated). The systems are neutralized with the addition of potassium or chloride ions. Water is represented by a blue surface, water molecules at less than 3 Å from any atom of the peptide or lipid bilayer are explicitly drawn in blue. DOPC and oleic acid molecules are shown with a white surface. Phosphate atoms are shown in yellow, protonated fatty acid carboxyl groups are shown in grey and the TAT is shown in red. In the bottom panel is shown the free energy profile as a function of the distance of the center of mass of the TAT peptide from the center of mass of the lipid bilayer. The total computed time for this free energy calculation profile expanded 10 μs.

Movie S2. Structures and free energy computation of the TAT peptide insertion into a phospholipid bilayer containing protonated and deprotonated fatty acids using molecular dynamics simulations. In the upper panel are shown molecular conformations of the systems with the peptide constrained along the direction perpendicular to the bilayer. The systems are composed of a TAT peptide, 8700 water molecules, 68 DOPC, 48 oleic acid molecules (24 protonated and 24 deprotonated). The systems are neutralized with the addition of potassium or chloride ions. Water is represented by a blue surface while water molecules at less than 3 Å from any atom of the peptide or lipid bilayer are explicitly drawn in blue. DOPC and oleic acid molecules are shown with a white surface. Phosphate atoms are shown in yellow, protonated (deprotonated) fatty acid carboxyl groups are shown in grey (green) and the TAT is shown in red. In the bottom panel is shown the free energy profile as a function of the distance of the center of mass of the TAT peptide from the center of mass of the lipid bilayer. The total computed time for this free energy calculation profile expanded 10 μs.

Movie S3. Structures and free energy computation of the TAT peptide insertion into a phospholipid bilayer containing deprotonated fatty acids using molecular dynamics simulations. In the upper panel are shown molecular conformations of the systems with the peptide constrained along the direction perpendicular to the bilayer. The systems are composed of a TAT peptide, 8700 water molecules, 68 DOPC, 48 oleic acid molecules (all deprotonated). The systems are neutralized with the addition of potassium or chloride ions. Water is represented by a blue surface, water molecules at less than 3 Å from any atom of the peptide or lipid bilayer are explicitly drawn in blue. DOPC and oleic acid molecules are shown with a white surface. Phosphate atoms are shown in yellow, protonated fatty acid carboxyl groups are shown in grey and the TAT is shown in red. In the bottom panel is shown the free energy profile as a function of the distance of the center of mass of the TAT peptide from the center of mass of the lipid bilayer. The total computed time for this free energy calculation profile expanded 10 μs.

Movie S4. Increasing the extracellular pH consistently increases the transduction efficiency of arginine rich peptides. Time-lapse fluorescence images show no cellular uptake of the TAT (2 μM) in living cells at pH 6. The upper image shows time-lapse confocal fluorescent images of the TAT peptide coupled to TAMRA and the lower DIC image captures the morphology of the cells. The images where acquired with a x20 objective magnification. Scale bar 75 μm.

Movie S5. Increasing the extracellular pH consistently increases the transduction efficiency of arginine rich peptides. Time-lapse fluorescence images show no cellular uptake of the TAT (2 μM) in living cells at pH 6. The upper image shows time-lapse confocal fluorescent images of the TAT peptide coupled to TAMRA and the lower DIC image captures the morphology of the cells. The images where acquired with a x60 objective magnification. Scale bar 15 μm.

Movie S6. Increasing the extracellular pH consistently increases the transduction efficiency of arginine rich peptides. Time-lapse fluorescence images show cellular uptake of the TAT (2 μM) in some living cells at pH 7.5. The upper image shows time-lapse confocal fluorescent images of the TAT peptide coupled to TAMRA and the lower DIC image captures the morphology of the cells. The images where acquired with a x20 objective magnification. Scale bar 75 μm.

Movie S7. Increasing the extracellular pH consistently increases the transduction efficiency of arginine rich peptides. Time-lapse fluorescence images show cellular uptake of the TAT (2 μM) in some living cells at pH 7.5. The upper image shows time-lapse confocal fluorescent images of the TAT peptide coupled to TAMRA and the lower DIC image captures the morphology of the cells. The images where acquired with a x60 objective magnification. Scale bar 15 μm.

Movie S8. Increasing the extracellular pH consistently increases the transduction efficiency of arginine rich peptides. Time-lapse fluorescence images show cellular uptake of the TAT (2 μM) in all living cells at pH 9. The upper image shows time-lapse confocal fluorescent images of the TAT peptide coupled to TAMRA and the lower DIC image captures the morphology of the cells. The images where acquired with a x20 objective magnification. Scale bar 75 μm.

Movie S9. Increasing the extracellular pH consistently increases the transduction efficiency of arginine rich peptides. Time-lapse fluorescence images show uptake of the TAT (2 μM) in all living cells at pH 9. The upper image shows time-lase confocal fluorescent images of the TAT peptide coupled to TAMRA and the lower DIC image captures the morphology of the cells. The images where acquired with a x60 objective magnification. Scale bar 15 μm.

Movie S10. Cells remain morphologically healthy and keep undergoing cell division after TAT peptide uptake at pH 9. Time-lapse fluorescence images show the TAT peptide (2 μM) after uptake at pH 9. The DIC image captures the morphology of the cells and cells undergoing division are encircled with dotted lines. The images where acquired with a x20 objective magnification every 30 min for 16 hours. Scale bar 75 μm.